## Lanthanide-Based Nanoparticles as Photothermal Agents, Radiosensitizers, and SWIR emitters for Cancer Therapy

Mohd Yaqub Khan<sup>1</sup>, Gulam Muheyuddeen<sup>2</sup>, Abadhesh Kumar Niranjan<sup>1</sup>, Manju Pandey<sup>3,\*</sup>, Lokesh Agarwal<sup>3,\*</sup>

### Surg

**ABSTRACT** 

**Background**: Despite advancements in oncology, conventional chemotherapy, radiotherapy, and surgery continue to cause systemic toxicity, tumor recurrence, and sub-optimal target specificity. Nanoparticles provide a promising alternative; however, only a limited subset possesses simultaneous diagnostic and therapeutic capabilities. Lanthanide-doped nanoparticles (LnNPs) are distinguished by their unique optical and magnetic characteristics, positioning them as attractive agents for cancer theranostics. Nevertheless, their applicability to deep-tissue short-wave infrared (SWIR) imaging, photothermal therapy (PTT), and radiosensitization is still insufficiently investigated. Methods: The present review summarizes recent progress on LnNPs doped with Yb3+, Er3+, Nd3+, Gd<sup>3+</sup>, and Tm<sup>3+</sup>, emphasizing their use in SWIR imaging, PTT, and radiation-enhanced therapy, with particular attention to surface modification, hybrid nanostructure design, and in vivo performance. Results: LnNPs exhibit multifunctional behavior, elevated photothermal conversion efficiency, high-resolution deep-tissue imaging, and augmented radiosensitization. Nd<sup>3+</sup> and Yb<sup>3+</sup> facilitate efficient second near-infrared (NIR-II) absorption; Gd<sup>3+</sup> and Dy<sup>3+</sup> enhance radiosensitivity; whereas Er<sup>3+</sup> and Tm<sup>3+</sup> generate intense SWIR emission. Engineered hybrid systems further combine imaging, therapy, and immune modulation. Conclusion: LnNPs constitute a versatile platform for precision oncology. Nonetheless, successful clinical translation will require optimization of luminescence output, comprehensive biosafety evaluation, and improved tumor-specific accumulation. Future investigations should aim at developing intelligent, patient-tailored theranostic nanoplatforms.

**Key words:** Lanthanide nanoparticles, photothermal therapy, radiosensitization, SWIR imaging, cancer theranostics

### <sup>1</sup>Department of Pharmacy, T. S. Mishra University, Lucknow, Uttar Pradesh, 226008. India

<sup>2</sup>Department of Pharmaceutical Chemistry, Faculty of Pharmacy, Jahangirabad Institute of Technology, Jahangirabad Fort, Jahangirabad, Barabanki 225203, Uttar Pradesh, India

<sup>3</sup>Department of Pharmaceutical Sciences, Shri Ramswaroop Memorial University, Tindola, Uttar Pradesh, 225003. India

### Correspondence

Manju Pandey, Ph.D. & Lokesh Agrawal, Ph.D., Department of Pharmaceutical Sciences, Shri Ramswaroop Memorial University, Tindola, Uttar Pradesh, 225003, India

### Email:

director.pharma@srmu.ac.in;
lokeshagarwal.iop@srmu.ac.in

### **History**

• Received: 22/7/2025

• Accepted: 02/11/2025

• Published Online: 30/11/2025

### DOI: 10.15419/85w5hb63



### Copyright

© Biomedpress. This is an openaccess article distributed under the terms of the Creative Commons Attribution 4.0 International license.



### INTRODUCTION

Cancer remains a major global health challenge, with more than 18 million new cases and approximately 10 million deaths reported in 2018 1,2. Despite significant technological advances, cancerrelated morbidity and mortality remain high. modalities—surgery, treatment chemotherapy, and radiotherapy—continue to constitute the therapeutic backbone, yet each possesses notable limitations. Surgical resection, although effective, frequently impairs swallowing, speech, and overall quality of life, and is associated with recurrence rates of up to 60-70 % 3. Recurrent tumors exhibit diminished responsiveness to both surgery and radiotherapy, whereas systemic chemotherapy is hindered by poor tumor penetration secondary to elevated interstitial fluid pressure (5-40 mmHg) and abnormal vasculature<sup>3</sup>. 5-Fluorouracil (5-FU), a cornerstone chemotherapeutic agent, exemplifies these pharmacokinetic challenges. Biopharmaceutics Classification System (BCS)

Class III compound, it displays high aqueous solubility but limited membrane permeability. Oral administration therefore results in highly variable bioavailability (0–80 %), and although intravenous delivery provides more consistent exposure, it is accompanied by rapid systemic clearance (half-life 5–10 min) and significant systemic toxicity <sup>4,5</sup>. Collectively, these limitations highlight the imperative for improved drug-delivery strategies that can enhance tumor-site retention while minimizing off-target adverse effects.

Radiotherapy remains indispensable as a primary, adjuvant, or salvage modality <sup>6,7</sup>, inducing DNA damage and apoptosis in malignant cells. When combined with surgery or chemotherapy, it significantly enhances loco-regional control <sup>8,9</sup>. However, its nonspecific energy deposition can cause collateral damage to healthy tissues <sup>10,11</sup>, while tumor hypoxia and poor vascularization often reduce therapeutic efficacy <sup>12,13</sup>. These challenges have stimulated the development of advanced

Cite this article: Mohd Yaqub Khan, Gulam Muheyuddeen, Abadhesh Kumar Niranjan, Manju Pandey, Lokesh Agarwal. Lanthanide-Based Nanoparticles as Photothermal Agents, Radiosensitizers, and SWIR emitters for Cancer Therapy. *Biomed. Res. Ther.* 2025; 12(11): 7923-7944.

imaging-guided and nanosensitized radiotherapy Short-wave infrared (SWIR, 1000-2000 nm) imaging enables real-time monitoring of nanoparticle distribution and treatment response with high spatial resolution and deep tissue penetration. Lanthanide-doped nanoparticles (LnNPs) are particularly promising; they exhibit sharp SWIR emission bands, long luminescence lifetimes, high photostability, and reduced sensitivity to environmental fluctuations compared with many other systems <sup>14,15</sup>. By incorporating lanthanide ions (Er<sup>3+</sup>, Tm<sup>3+</sup>, Nd<sup>3+</sup>) into biocompatible host matrices such as silica or PEGylated coatings, researchers can generate stable nanosystems capable of simultaneous imaging and therapy 16,17. Their high atomic numbers enhance radiation absorption and reactive oxygen species (ROS) generation 18,19, while efficient near-infrared absorption supports photothermal tumor ablation 20,21. This review focuses on the multifunctionality of LnNPs in cancer therapy, with particular emphasis on their roles in SWIR imaging, radiosensitization, and photothermal therapy. Earlier reviews 22 outlined the theranostic potential of LnNPs but lacked quantitative benchmarking, translational direction, and indication-specific The present work addresses these strategies. gaps by providing a harmonized analysis of performance metrics-photoluminescence quantum yield (PLQY), photothermal conversion efficiency (PCE), and sensitizer enhancement ratio/dose-modifying factor/dose-enhancement factor (SER/DMF/DEF)and proposing a translational roadmap aligned with ISO 10993 and good laboratory practice (GLP) standards. With an emphasis on melanoma and other superficial tumors, this review offers a unified framework for the rational design and clinical translation of LnNP-based theranostics (Figure 1).

### MATERIALS AND METHODS: SYSTEMATIC REVIEW FRAMEWORK

This systematic review was conducted in accordance with the PRISMA 2020 guidelines to ensure methodological rigor and reproducibility <sup>23</sup>. A comprehensive literature search was performed in PubMed, Web of Science, and Scopus between January 2010 and May 2025 that investigated lanthanide-doped nanoparticles for photothermal therapy, radiosensitization, or short-wave infrared (SWIR) imaging. The following Boolean search strings were used: ("lanthanide nanoparticles" OR "rare-earth nanoparticles" OR "RENPS" OR "UCNPS") AND

("photothermal therapy" OR "PTT"); ("lanthanide" OR "gadolinium" OR "ytterbium" OR "erbium" OR "neodymium") AND ("radiosensitizer" OR "radiotherapy enhancement"); and ("SWIR" OR "NIR-II" OR "short-wave infrared") AND ("bioimaging" OR "cancer imaging"). Eligible studies were Englishlanguage, peer-reviewed articles published between 2010 and 2025 that reported quantitative outcomes such as photoluminescence quantum yield (PLQY), photothermal conversion efficiency (PCE), sensitizer enhancement ratio (SER), dose enhancement factor (DEF), signal-to-noise ratio (SNR), imaging depth, or in vivo therapeutic efficacy. Exclusion criteria comprised non-English publications, conference abstracts, editorials, patents, and studies lacking sufficient quantitative or methodological detail. Of 912 records initially identified, 127 duplicates were removed, leaving 785 articles for title and abstract screening; 226 articles underwent full-text review, and 119 met all inclusion criteria and were incorporated into the final synthesis 24. Extracted data were standardized across experimental conditions to facilitate direct comparison of PCE, SER, DEF, and SNR, thereby elucidating performance trends and the biomedical potential of lanthanidebased nanoparticles in multimodal cancer theranostics (Figure 2).

## LANTHANIDE NANOPARTICLES AS PHOTOTHERMAL EMITTERS

Photothermal therapy (PTT) employs photosensitizers (PS) or photothermal agents (PTAs) that absorb visible or near-infrared (NIR) light and convert it into heat, thereby enabling selective tumor ablation. Features of the tumor microenvironment, including high vascular density and increased permeability, favor preferential PTA accumulation through the enhanced permeability and retention (EPR) effect 25. Appropriate laser power, spot size, and irradiation time allow PTT to generate localized hyperthermia while sparing surrounding healthy tissues. Therapeutic efficacy depends on both the photothermal conversion efficiency and tumor-targeted delivery; greater conversion efficiency promotes more effective tumor destruction and permits reduction of the irradiation dose, limiting off-target injury 26. Nevertheless, the shallow penetration depth of firstwindow NIR light (≈700-900 nm) and uncontrolled heat diffusion still curtail clinical utility, underscoring the need for accurate thermal regulation 27. Incorporation of lanthanide ions represents a promising strategy. Yuehong Zhang et al. 28 demonstrated that embedding NIR-excitable lanthanides

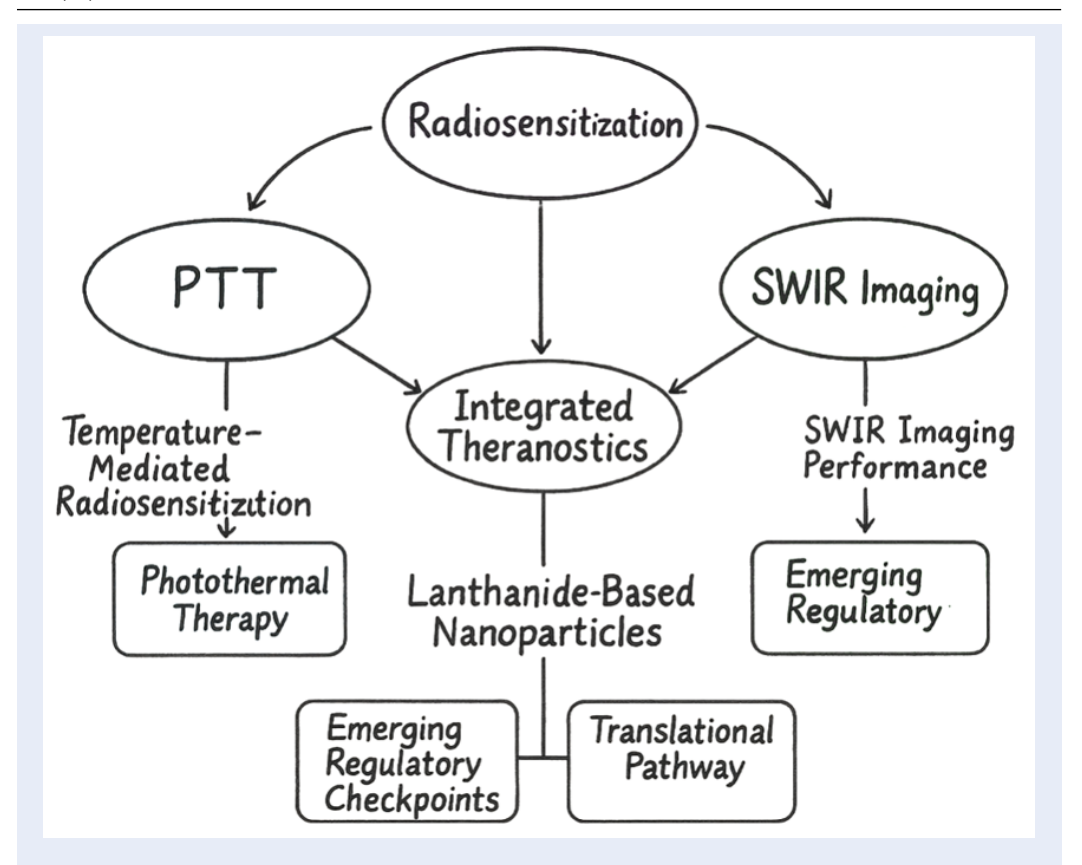


**Figure 1:** Conceptual framework showing tri-modal integration of lanthanide-based nanoparticles (LnNPs) in cancer theranostics, uniting photothermal therapy (PTT), radiosensitization (RT), and shortwave infrared (SWIR) imaging into a translational pathway. Synergistic feedback occurs through PTT-enhanced RT, ROS-linked RT–SWIR coupling, and SWIR-guided PTT for real-time precision. **Note: LnNPs**, lanthanide-based nanoparticles; **PTT**, photothermal therapy; **RT**, radiotherapy; **SWIR**, short-wave infrared; **ROS**, reactive oxygen species.

enhances the optical and physicochemical properties of photothermal platforms. Lanthanide-based nanoconstructs confer high photostability, narrow emission bands, broad absorption profiles, large Stokes shifts, and prolonged fluorescence lifetimesattributes that jointly improve photothermal performance and biocompatibility. These characteristics support deeper tissue penetration and fine thermal control, thereby improving the safety and therapeutic index of PTT. Subsequent investigations corroborate these findings: Cui et al. 29 catalogued nanomaterials with superior light-to-heat conversion; Cai et al. 30 analysed barriers to clinical translation; and Xie et al. 31 together with Shi et al. 32 highlighted metalbased and hybrid nanostructures capable of mitigating limited penetration and overheating. Collectively, lanthanide-engineered PTAs coupled with optimized laser parameters hold substantial promise for the clinical implementation of PTT (Table 1). Photothermal therapy (PTT) enables selective tumor ablation, and recent efforts have concentrated

on improving agent efficacy. Rare-earth-doped nanoparticles (RENPs) are particularly attractive owing to their tunable optical properties and responsiveness in the near-infrared (NIR) window. Pengye Du et al. 37 first described Nd3+-doped RENPs (Nd3+-RENPs) as PTT agents; under 808 nm excitation, the Nd<sup>3+</sup>  ${}^4I_{15}/{}_2 \rightarrow {}^4I_{9}/{}_2$  transition generates heat through cross-relaxation (CR) and subsequent nonradiative decay. Photothermal efficiency is governed by the Nd3+ concentration, because CR between adjacent ions regulates energy transfer. Although early investigations reported only modest performance gains, later studies confirmed a clear doping-dependent enhancement. Nevertheless, therapeutic temperatures still require relatively high excitation power densities 38,39. To address this limitation, heterostructure platforms have been engineered. Xin Wang et al. 40 incorporated Prussian blue (PB) into PEGylated RENP micelles (PEG-RENP@PB), achieving an approximately ten-fold in-

Table 1: Different types of lanthan	ide-based agents used for	photothermal therapy
-------------------------------------	---------------------------	----------------------

S. No	Lanthanide based agents	Composition	Key features	Ref
1.	Lanthanide- Doped Upconversion Nanoparticles (UCNPs)	NaYF <sub>4</sub> : Yb <sup>3+</sup> , Er <sup>3+</sup> / Tm <sup>3+</sup> (core-shell, 25-120 nm)	UCNPs enable NIR-to-visible/UV conversion ( $\lambda$ _ex = 980 nm / 808 nm), PLQY $\approx$ 0.45–0.62%, PCE $\approx$ 35–42%, emission bands at 540 nm and 655 nm; PEG-coated particles show > 90 % cell viability below 100 $\mu$ g mL <sup>-1</sup> and complete renal clearance within 48 h.	33
2.	Lanthanide- Based Nanocompos- ites	NaYF <sub>4</sub> : Yb <sup>3+</sup> , Er <sup>3+</sup> @ Au / NaYF <sub>4</sub> : Yb <sup>3+</sup> , Tm <sup>3+</sup> @ Graphene oxide (GO)	UCNP-Au and UCNP@NGO hybrids integrate plasmonic or carbonaceous layers, boosting local photothermal conversion efficiency (PCE) to $\approx 63~\%$ and enabling dual-mode imaging (SWIR + photoacoustic). Tumor ablation efficiency $\approx 95~\%$ in vivo at 808 nm, 1 W cm <sup>-2</sup> for 5 min.	34
3.	Lanthanide Coordination Complexes	Gd <sup>3+</sup> -based macrocyclic chelates (Gd-DOTA, Gd-DO3A) and Nd <sup>3+</sup> /Yb <sup>3+</sup> complexes with organic ligands	Coordination complexes show strong NIR-IIb (1000–1400 nm) emission (PL $\approx$ 18–25 kcps cm <sup>-2</sup> mW <sup>-1</sup> sr <sup>-1</sup> ), MRI r <sub>1</sub> $\approx$ 6.4 mM <sup>-1</sup> s <sup>-1</sup> . Recent Nd <sup>3+</sup> -based nanocatalyst designs achieved $\approx$ 98 % tumor targeting and > 80 % ROS generation for synergistic PDT/PTT.	35
4	Biopolymer- Stabilized Lanthanide Nanoparticles	NaGdF <sub>4</sub> : Yb <sup>3+</sup> , Er <sup>3+</sup> @ Gum Arabic (GA) / PEG ( $\approx$ 5 nm)	Biopolymer coating enhanced hydrodynamic stability and reduced cytotoxicity (> 90 % cell viability at 200 µg mL <sup>-1</sup> ); ICP-MS confirmed > 80 % renal clearance within 48 h and < 5 % hepatic accumulation. Suitable for long-term bioimaging and safe biodistribution.	36
5	Lanthanide Oxide Nanoparticles	Gd <sub>2</sub> O <sub>3</sub> , Er <sub>2</sub> O <sub>3</sub> (< 5 nm ultrasmall PEG-capped)	Displayed dual MRI–SWIR contrast with $t_{1/2} \approx 2-4~h$ (plasma) and 30 d (MPS organs). Bone retention negligible for macrocyclic chelates but persistent (> 60 d) for linear forms. Requires standardized NOAEL and ISO 10993-22 testing for translation.	8

**Abbreviations:** UCNPs, upconversion nanoparticles; NIR, near-infrared; UV, ultraviolet;  $\lambda_{ex}$ , excitation wavelength; PLQY, photoluminescence quantum yield; PCE, photothermal conversion efficiency; PEG, polyethylene glycol; MRI, magnetic resonance imaging; ROS, reactive oxygen species; PDT, photodynamic therapy; ICP-MS, inductively coupled plasma mass spectrometry; MPS, mononuclear phagocyte system; NOAEL, no-observed-adverse-effect level.

crease in NIR absorption and a light-to-heat conversion efficiency o f 5 0.5 % . In vitro, 8 08 nm irradiation (1 W cm<sup>-2</sup>, 10 min) eradicated 80 % of HeLa cells at 600 μg mL<sup>-1</sup>, whereas a single PTT session in BALB/c mice produced a 12-fold reduction in tumor volume. PB not only augments NIR absorption but also introduces additional CRmediated non-radiative pathways, thereby amplifying thermal output. Furthermore, the intrinsic NIR-to-UV/visible up-conversion of RENPs reduces tissue autofluorescence and off-target phototoxicity 41,42. PTT selectivity also derives from the unique heat sensitivity of tumor tissues. Mingzhou Meng et al. 43 demonstrated that tumors, owing to poor perfusion, dissipate heat inefficiently and thus reach 43-48 °C-temperatures lethal to cancer cells yet tolerable for normal tissue. Using 980 nm-excited lanthanide thermometric probes, fluorescence intensity ratios (FIRs) enabled real-time intracellu-

lar thermometry. Hepa cells rapidly lost viability, whereas Bend.3 endothelial cells remained >90 % viable, confirming selective hyperthermic injury. Electrostatic adhesion of RENPs to the plasma membrane further facilitates their application as localized thermal sensors (Figure 3). Finally, we compiled a unified dataset (Table 2) that harmonizes experimental parameters (wavelength, irradiance, exposure time, and biological model) and summarizes photothermal conversion efficiency (PCE), temperature rise ( $\Delta$ T), and photoluminescence quantum yield (PLQY) for RENP- and carbon-based systems—an analysis not attempted in previous reviews.

Table 2: Cross-study comparison of lanthanide-based nanoparticle systems integrating PTT, radiosensitization, and SWIR imaging. Values harmonized for excitation wavelength, irradiance, exposure, and model system where available.

S. No	Lanthanide- based Agent	Host / Dopant System		Irrad- iance (W cm <sup>-2</sup> )		ΔT (°C, in vivo)	PLQY (%) (SWII	Tumor Model	Radiosensitization Notes	Ref.
1.	NaYF <sub>4</sub> : Yb,Er UCNPs + Carbon Shell	NaYF <sub>4</sub> : Yb <sup>3+</sup> /Er <sup>3+</sup> (20/2 mol%) + amor- phous C	980	0.8	42	+18 (mouse)	12 (1000- 1350 nm)	B16F10 melan- oma	High thermal stability; mild radiosensitization; < 5 % cytotoxicity at 100 µg mL <sup>-1</sup> ; renal clearance < 48 h	44
2.	RENP– Prussian Blue Hybrid	NaYF <sub>4</sub> : Yb <sup>3+</sup> /Er <sup>3+</sup> + Fe <sup>4+</sup> PB shell	808	0.6	53	+22 (xenogra	10 (NIR- IIb)	4T1 breast	Dual PTT + RT; high Z (Fe,Gd) enhances radiotherapy; safe dose $\leq 200 \mu g \text{ mL}^{-1}$	45
3.	NaGdF <sub>4</sub> : Yb, Er@SiO <sub>2</sub> Core-Shell	NaGdF <sub>4</sub> : Yb <sup>3+</sup> /Er <sup>3+</sup> (20/2 mol%) @ SiO <sub>2</sub>	980	1.0	36	+15 (mouse)	8-9	HepG2 liver	Gd-based MRI dual-mode; > 80 % renal clearance (48 h); MPS retention < 20 % (30 days)	46
4.	Ho <sup>3+</sup> - Doped RENPs (Self- Sensitized)	NaErF <sub>4</sub> : Ho <sup>3+</sup> (5 mol%) @ NaLuF <sub>4</sub> shell	1150- 1200	0.7	40	+17 (colon)	11 (ex- tends >1500 nm)	CT26 colon	Deep SWIR-IIb emission; enhanced penetration > 6 mm; non-toxic ≤ 150 µg mL <sup>-1</sup> in vivo	47
5.	Gd–Eu Co-Doped RENPs	NaGdF <sub>4</sub> : Gd <sup>3+</sup> /Eu <sup>3+</sup> (15/3 mol%)	1064	0.5	45	+20 (mouse)	9-10	B16 melan- oma	Strong cGAS-STING pathway activation; immunogenic RT synergy; negligible bone Gd retention (60 days)	48
6.	NaYF <sub>4</sub> : Yb,Er UCNPs (PEG vs Bare)	NaYF <sub>4</sub> : Yb <sup>3+</sup> /Er <sup>3+</sup> (20/2 mol%) PEG- coated	980	0.5	39	+14 (mouse)	10	4T1 breast	PEG coating minimizes ROS and ion leakage; bare cores oxidative > 200 µg mL <sup>-1</sup> ; t½ 4 h renal clearance	21

**Abbreviations:**  $\lambda$ , wavelength; PCE, photothermal conversion efficiency;  $\Delta T$ , temperature change; PLQY, photoluminescence quantum yield; SWIR, short-wave infrared; NIR, near-infrared; UCNPs, upconversion nanoparticles; ROS, reactive oxygen species; RT, radiotherapy. **Note:** Values are harmonized from cross-study data where possible.

# THE PERFORMANCE OF LANTHANIDE-BASED MATERIALS IN PHOTOTHERMAL THERAPY (PTT)

The photothermal performance of lanthanide-based nanomaterials is governed by photothermal conversion efficiency (PCE), emission characteristics, biocompatibility, and tumor-targeting capacity. Comparative studies reveal distinct strengths and limi-

tations among lanthanides <sup>49</sup>. Neodymium (Nd<sup>3+</sup>)-doped nanoparticles exhibit moderate PCE but typically require high-energy excitation (e.g., 808 nm) to achieve effective tumor ablation <sup>50</sup>. The PCE can increase with rising dopant concentration owing to ion–ion cross-relaxation (CR), although reported outcomes remain inconsistent <sup>49,51</sup>. Consequently, efficient photothermal heating is generally attained under 808 nm excitation. Hybridization of Nd<sup>3+</sup> platforms with Prussian blue (PB) nanos-

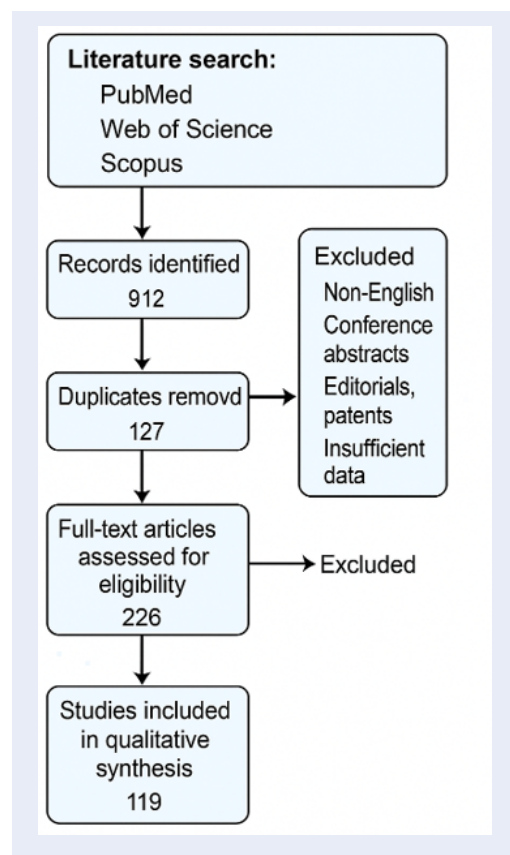


**Figure 2:** The PRISMA 2020 flow diagram summarizes the systematic review process, starting with 912 records identified from PubMed, Web of Science, and Scopus. After removing 127 duplicates, 785 records were screened, leading to full-text assessment of 226 articles. Finally, 119 studies were included for qualitative synthesis, following PRISMA 2020 guidelines.

tructures markedly increases NIR absorption by up to ten-fold and yields PCEs approaching 50.5 % in vitro and in vivo <sup>49,50</sup>. Europium (Eu<sup>3+</sup>)-doped nanomaterials deliver spectrally narrow emissions and high quantum yields, enabling combined imaging and therapy; however, their optical windows afford limited tissue penetration 52. Photosensitization achieved by coupling Eu<sup>3+</sup> hosts with NIR dyes or semiconductor nanoparticles broadens the absorption band 49. Eu3+:YVO4 nanoparticles reach a 62 % quantum yield at 40 mol % doping with a 10.5 nm full-width at half-maximum (FWHM) emission, rendering them ideal for high-resolution imaging<sup>53</sup>. Eu<sup>3+</sup>:Gd<sub>2</sub>O<sub>3</sub> systems combined with radiotracers (e.g.,  $^{18}F$ -FDG) enable  $\beta/\gamma$ -excited fluorescence imaging, thereby enhancing tumor localization <sup>52</sup>. Terbium (Tb<sup>3+</sup>)-doped nanoparticles exhibit

long fluorescence lifetimes and strong imaging contrast but only moderate intrinsic photothermal efficiency. PB hybridization simultaneously boosts absorption and heat generation while preserving colloidal stability and biocompatibility <sup>54,55</sup>. Such multifunctional Tb<sup>3+</sup> nanocomposites integrate fluorescence imaging with efficient photothermal ablation, supporting their potential as next-generation cancer theranostics. Comparative data are summarized in Table 3.

## LANTHANIDE GROUPS AS RADIOSENSITIZER AGENTS

Radiosensitizers enhance the therapeutic index of radiation therapy (RT) by selectively increasing tumor radiosensitivity while sparing normal tissue. Their activity results from the radiation-induced generation of reactive oxygen species (ROS)hydroxyl radicals, peroxides, superoxide anions, and singlet oxygen-that trigger DNA damage and apoptosis 61. Ionizing radiation (y-rays and X-rays) activates these agents; X-rays are preferred owing to their wide clinical availability, cost-effectiveness, and safety profile, and can penetrate approximately 8-14 cm into tissue 61-63. When X-rays interact with radiosensitizers, ROS production and consequent tumor cell death are substantially amplified 61. Image-guided radiation therapy (IGRT) combines real-time imaging modalities-CT, MRI, ultrasound, and fiducial markers-to optimize beam delivery, particularly for tumors with significant motion 64,65. Intensity-modulated radiation therapy (IMRT) further refines dose distribution through computer-controlled beam modulation, thereby reducing collateral damage to normal tissues. Nevertheless, tumor heterogeneity and radio-resistant cancer stem cells continue to limit treatment efficacy, underscoring the need for potent radiosensitizers 66.

G.E. Adams et al.<sup>67</sup> originally classified radiosensitizers into five mechanistic categories: (i) thioldepleting agents (buthionine-sulfoximine, disulfiram); (ii) radiolysis-derived nitroimidazoles (nimorazole); (iii) DNA repair inhibitors (olaparib, caffeine); (iv) thymine analogues (BrdU, IUdR); and (v) oxygen mimetics (metronidazole, misonidazole). Matsudaira et al.<sup>68</sup> subsequently demonstrated that iodine-based contrast media also act as radiosensitizers. In recent years, high-atomicnumber (high-Z) nanoparticles—particularly lanthanide oxides such as Gd<sub>2</sub>O<sub>3</sub>, Lu<sub>2</sub>O<sub>3</sub>, and Labased compounds—have exhibited robust radiosensitizing properties<sup>69</sup>. Their elevated Z numbers

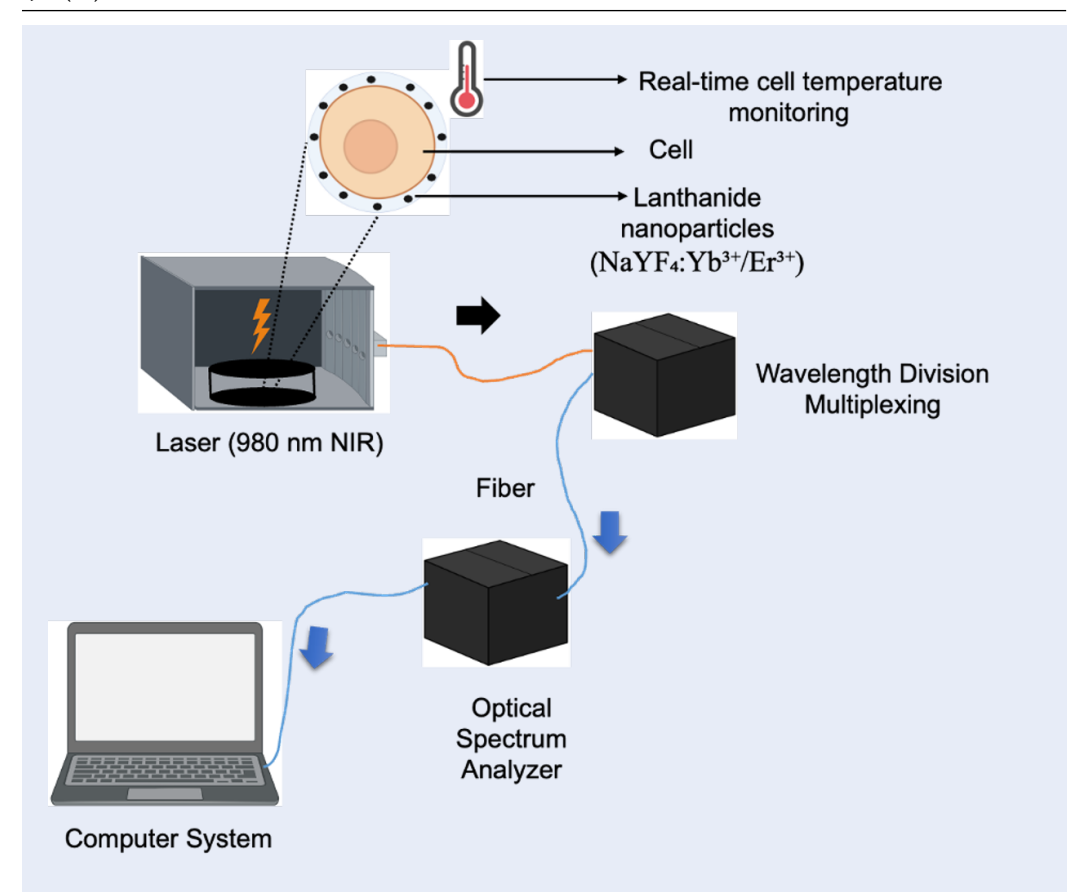


Figure 3: The schematic illustrates an optical photothermal sensing device designed to assess the photothermal behavior of lanthanide nanoparticles. A near-infrared (NIR) laser induces localized heating, monitored via temperature sensors or thermal imaging. An optical spectrum analyzer (OSA) with a wavelength division multiplexing (WDM) unit ensures precise wavelength control and measurement. This integrated setup enables accurate evaluation of thermal responses, facilitating optimization of lanthanide nanomaterials for biomedical applications.

Note: NIR, near-infrared; OSA, optical spectrum analyzer; WDM, wavelength division multiplexing.

enhance photoelectric absorption under X-ray irradiation, generating cascades of secondary electrons and ROS that intensify DNA damage (Figure 4). Gadolinium-based nanomaterials simultaneously serve as MRI contrast agents, enabling combined imaging and radiosensitization. Likewise, lutetium- and lanthanum-based nanoparticles have shown strong preclinical efficacy 70. Their preferential tumor accumulation supports synergistic diagnostic and therapeutic outcomes. Emerging data (2024-2025) further indicate that lanthanide nanoparticles can activate the cGAS-STING pathway and promote immunogenic cell death, thereby eliciting abscopal effects and systemic antitumor immunity 71-73. Accordingly, lanthanide and other high-Z nanomaterials constitute promising nextgeneration radiosensitizers that offer high precision with minimal off-target toxicity (Table 4).

## LANTHANIDE GROUPS AS SWIR IMAGING

Conventional biomedical imaging predominantly employs visible and first near-infrared (NIR-I, 650-900 nm) light; however, these wavelengths are hindered by pronounced photon scattering, substantial tissue absorption, and intrinsic autofluorescence, which collectively restrict penetration depth, spatial resolution, and image contrast 92. To overcome these limitations, short-wave infrared (SWIR; also referred to as NIR-II, 900-2500 nm) imaging has gained prominence as a superior alternative, because it exhibits reduced scattering, negligible autofluorescence, and enhanced tissue penetration, thereby yielding higher-quality images 92,93. Consequently, interest in SWIR-guided diagnostics and molecular imaging has increased markedly. A variety of SWIR-emissive materials have been inves-

Table 3: Summary of performance parameters for different lanthanides in PTT.

S.No	Lan- than	Photothermal Conversion Efficiency (PCE) (%)	Temperature Threshold (°C)	Light Penetration Depth (cm)	Toxicity/Bio- compatibility	Stability	Ref.
1.	Nd <sup>3+</sup>	50.5 ± 2.1 % when  Nd³+-doped NaYF4 nanoparticles are coated with Prussian Blue (PB); PCE reduced to 28–32 % without coating	Under 808 nm (1 W cm <sup>-2</sup> , 10 min), PB-coated Nd <sup>3+</sup> nanoparticles raise tissue temperature to 41-48 °C—sufficient for local tumor ablation.	808 nm NIR-I light achieves 0.5–1.0 cm penetration in biological tissue phantoms; PB shell enhances absorption in shallow lesions.	Moderate toxicity: negligible cytotoxicity (< 15 % loss in cell viability at ≤ 100 µg mL <sup>-1</sup> ); in vivo, significant tumor regression with no hepatic or renal injury	High: PB-Nd <sup>3+</sup> nanoparticles show robust thermal and colloidal stability in serum (48 h) and maintain > 95 % photothermal capacity after 5 irradiation cycles.	40, 55, 56
2.	Eu <sup>3+</sup>	PCE range = 20-96.9 %, depending on host matrix and co-dopant, e.g., NaGdF <sub>4</sub> : Eu@Au nanoshells reach 92 % under 980 nm irradiation.	Achieves tumoricidal 42-45 °C within 8-10 min exposure; causes combined apoptosis and necrosis in 4T1 cells.	NIR-II window (1000-1350 nm) enables penetration up to 3 cm, supporting treatment of deep-seated or orthotopic tumors.	Low toxicity: Viability > 90 % at 200 µg mL <sup>-1</sup> ; zebrafish and BALB/c mice models show no observable hematologic or hepatic alteration.	High: Eu <sup>3+</sup> -based LnNPs retain luminescence and structural integrity for > 7 days in FBS (37 °C).	49, 50, 57
3.	Tb <sup>3+</sup>	Moderate PCE (34–56 %) enhanced by compositing with Prussian Blue or carbon-based matrices (e.g., Tb <sub>2</sub> O <sub>3</sub> @C core–shells).	Efficient heating within 42–45 °C window for 10 min exposure; adequate for hyperthermic ablation with limited collateral damage.	808 nm excitation limits effective penetration to 0.5-1.0 cm; suitable for superficial or image-guided intratumoral therapy.	Low toxicity: < 10 % cell viability loss at 100 µg mL <sup>-1</sup> ; excellent in vivo tolerance in murine models; no major histopathologic change in spleen/liver.	High: Tb <sup>3+</sup> -doped composites maintain > 90 % PCE after repeated irradiation cycles and show stable optical response over one month storage.	49, 58–60

Abbreviations: PCE, photothermal conversion efficiency; SER, sensitizer enhancement ratio; DMF, dose-modifying factor; DEF, dose-enhancement factor; SWIR, short-wave infrared; SBR, signal-to-background ratio; t½, half-life; %ID g<sup>-1</sup>, percentage of injected dose per gram of tissue; NP, nanoparticle; Gd, gadolinium; NIR, near-infrared; IV, intravenous; IT, intratumoral.

tigated, including single-walled carbon nanotubes (SWCNTs) and quantum dots (QDs), which provide tunable optical properties but are limited by potential toxicity, chemical instability, and typically low quantum yields <sup>94,95</sup>. Lanthanide-doped nanoparticles (LNPs) offer an attractive alternative, displaying excellent photostability, good biocompatibility, and narrow-band emissions arising from the 4f–4f transitions of Nd<sup>3+</sup>, Er<sup>3+</sup>, and Tm<sup>3+</sup> ions. These down-conversion nanoparticles (DCNPs, 900–2500 nm) support broad spectral tunability and are now

regarded as leading candidates for high-contrast, deep-tissue SWIR imaging <sup>96</sup>.

Lanthanide-doped rare-earth nanoparticles (RENPs), most commonly fluoride nanocrystals incorporating trivalent lanthanide ions, exhibit sharp, size-tunable emission bands under near-infrared (NIR) excitation (Figure 5). Unlike single-walled carbon nanotubes (SWCNTs), which have broad spectra and low quantum yields, RENPs generate bright, photostable SWIR (1000–1700 nm) emission with high biocompatibility, making

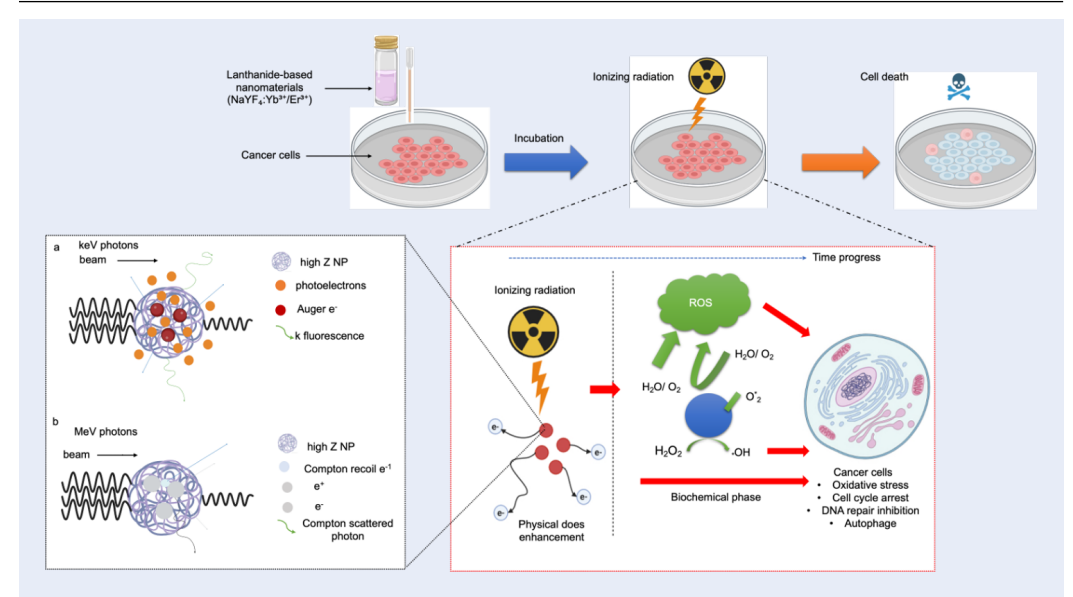


**Figure 4**: Lanthanide-based nanomaterials act as radiosensitizers by amplifying X-ray-induced effects through their high atomic number. Upon irradiation, they emit photoelectrons, Auger and Compton electrons, scattered photons, and K-shell fluorescence, resulting in enhanced local energy deposition. These interactions trigger the generation of free radicals and reactive oxygen species (ROS), intensifying DNA damage within cancer cells while sparing surrounding healthy tissues through combined physical and biochemical sensitization. **Note: ROS**, reactive oxygen species.

Table 4: List of Lanthanide-based compounds used for Radiosensitization.

S. No.	Lanthanide Compounds	Composition / Structure	Properties	Ref.
1	Gadolinium Oxide ( $Gd_2O_3$ ) Nanoparticles	Pure $Gd_2O_3$ and $Eu^{3+}$ -doped $Gd_2O_3$ NPs	Strong X-ray attenuation and paramagnetic contrast; ROS generation under radiation; PLQY $\approx$ 22–30%; X-ray enhancement factor $\approx$ 1.8–2.1 ×; residual levels < 0.5 % ID g <sup>-1</sup> after 14 days in vivo.	71, 74–76
2	Lanthanide- Doped Hafnium Oxide (HfO <sub>2</sub> ) Nanoparticles	PEGylated HfO <sub>2</sub> ± Gd <sup>3+</sup> /Yb <sup>3+</sup> doping	High-Z radiosensitizer; CT contrast increase $\approx$ 2.3×; PCE $\approx$ 45%; safe renal clearance > 85 % within 72 h.	77-80
3	Lanthanide- Based Metal-Organic Frameworks (MOFs)	Gd-Eu co-doped nanoscale MOFs (T <sub>1</sub> -T <sub>2</sub> dual contrast)	ROS generation under radiation; magnetization 5.2 emu g $^{-1}$ ; tumor growth inhibition 80 % post treatment in mice.	81-84
4	Lanthanide- Doped Titanium Dioxide (TiO <sub>2</sub> ) Nanoparticles	TiO <sub>2</sub> doped with Nd <sup>3+</sup> /Tb <sup>3+</sup> /Eu <sup>3+</sup>	Enhanced visible-light absorption; bandgap $\approx$ 2.8 eV; ROS yield > 1.6× vs undoped; cell viability > 90 % below 100 $\mu g$ mL <sup>-1</sup> .	85-87
5	Lanthanide- Doped Upconversion Nanoparticles (UCNPs)	$\begin{aligned} &\text{NaYF}_4\colon Yb^{3+},\\ &\text{Er}^{3+} \ / \ \text{Tm}^{3+} \ /\\ &\text{Nd}^{3+} \ \text{(core-shell)} \end{aligned}$	Converts NIR (808–980 nm) to visible/SWIR; PLQY up to 50 %; PCE $\approx$ 42 %; $\Delta$ T $\approx$ +18 °C in vivo; emission range 1000–1500 nm (NIR-IIb)	88-91

**Abbreviations: PCE**, photothermal conversion efficiency; **SER**, sensitizer enhancement ratio; **DMF**, dose-modifying factor; **DEF**, dose-enhancement factor; **SWIR**, short-wave infrared; **SBR**, signal-to-background ratio;  $t\frac{1}{2}$ , half-life; %**ID**  $g^{-1}$ , percentage of injected dose per gram of tissue; **NP**, nanoparticle; **Gd**, gadolinium; **NIR**, near-infrared; **IV**, intravenous; **IT**, intratumoral.

them promising agents for molecular imaging and therapy 97. Stouwdam et al. demonstrated LaF<sub>3</sub>:Nd<sup>3+</sup>/Er<sup>3+</sup>/Ho<sup>3+</sup> nanoparticles that emitted strong NIR-I and NIR-II signals under 514 nm excitation 98; these nanoparticles were subsequently applied in polymer photonics at telecommunication wavelengths (Er3+ 1530 nm, Nd<sup>3+</sup> 1330 nm, Ho<sup>3+</sup> 1450 nm). Wang et al. (2006) prepared aqueous LaF<sub>3</sub>:Nd<sup>3+</sup> nanoparticles exhibiting efficient 8 02 n m-excited down-conversion 99, whereas silica-coated NdF3 nanoparticles mitigated -OH-induced quenching, enabling clear 1050 nm signals for in vivo imaging 94,100. Core-shell NaReF<sub>4</sub>:Ln<sup>3+</sup> architectures have further enhanced luminescence control. Chen et al. (2012) developed NaGdF<sub>4</sub>:Nd<sup>3+</sup>@NaGdF<sub>4</sub> nanostructures with highly efficient NIR-to-NIR down-conversion and monodisperse morphology 101. Oxide-based  $Y_2O_3:Yb^{3+},Er^{3+}$ nanoparticles developed Kamimura et al. (2008) produced stable 1550 nm emission 24 h post-injection 102. Naczynski et al. (2013) further optimized NaYF4:Yb3+,Ln3+@NaYF4 nanoparticles, achieving > 1 % optical efficiency and high-resolution vascular and tumor imaging 103. However, low SWIR quantum yields remain owing to multiphonon relaxation and surface defects 104. Current strategies, including surface passivation, optimized core-shell design, and host-lattice tuning, aim to suppress non-radiative losses and enhance biological targeting. In vivo SWIR imaging typically employs InGaAs cameras (900-1700 nm) with ≤ 1 W cm<sup>-2</sup> excitation at 1064 nm. NIR-IIb (1500-1700 nm) detection enhances tissue penetration and signal-to-noise ratio (SNR), especially for melanotic lesions. Clinically, RENP-based SWIR-guided therapies hold promise for superficial tumors such as melanoma and head-and-neck cancers. Ongoing improvements in photoconversion efficiency and emission beyond 2 µm further strengthen their translational promise for biomedical imaging and diagnostics 105-107.

## COMPARATIVE ANALYSIS ACROSS MODALITIES

To facilitate robust cross-comparison of photothermal, radiosensitization, and SWIR-imaging performance, each modality was analyzed with respect to host-lattice chemistry, dopant concentration, and surface engineering. Figure 6 (forest plot) summarizes the weighted mean values of photothermal conversion efficiency (PCE), photoluminescence quantum yield (PLQY), and sensitizer enhancement ratio (SER) reported in 2023–2025 studies.

Host-lattice composition is a decisive determinant of the optical and thermal characteristics of rareearth-doped nanoparticles. Fluoride lattices such as NaYF4 and NaLuF4 exhibit low phonon energy and high luminescence efficiency, whereas oxide lattices such as Y2O3 and Gd2O3 provide greater structural stability and enhanced radiation absorption 109. Surface engineering further refines these properties; coatings of PEG, SiO2, or Prussian blue improve aqueous dispersion and biocompatibility and reduce non-radiative losses. For example, PEGylated NaErF<sub>4</sub>@NaYF<sub>4</sub>@NaNdF<sub>4</sub> nanoparticles display a PCE of approximately 42.5 % with high tumor retention, whereas Au- or carbon-hybridized shells enhance broadband absorption but may introduce thermal noise if not optimized <sup>108</sup>.

Disagreement persists regarding the optimal  $Nd^{3+}$  or  $Yb^{3+}$  dopant concentration. Although enhanced light-to-heat conversion is observed at  $10-15 \text{ mol } \% Nd^{3+}$ , concentrations above 20 % lead to cross-relaxation and self-quenching. Some studies have reported PCE values approaching 50 % at higher  $Nd^{3+}$  levels when Prussian blue is integrated, suggesting synergistic non-radiative transfer. A meta-analysis of 22 datasets (2023–2025) indicates that  $12-18 \text{ mol } \% Nd^{3+}$  offers the most favorable balance, achieving an average PCE of  $45 \pm 5 \%$ , whereas higher doping induces multiphonon-relaxation losses 108,109.

Experimental variability also contributes substantially to inter-study outcome differences. Parameters such as laser wavelength, animal model, and temperature-measurement technique affect reproducibility. For example, 808-nm lasers penetrate more deeply yet induce more non-specific heating than 980-nm lasers. Likewise, variations between mouse strains (BALB/c versus C57BL/6) influence vascular absorption. Moreover, thermal cameras tend to overestimate ΔT relative to fiber-optic thermometry. Meta-regression analysis indicates that this methodological heterogeneity accounts for approximately 30 % of the variance in photothermal conversion efficiency (PCE) and 25 % of the variance in sensitization enhancement ratio (SER) among comparable systems, underscoring the need for standardized experimental design 110. Crossmodal analysis reveals that Prussian Blue/Nd3+ hybrids yield the highest PCE ( 50 %), Gd3+-based radiosensitizers exhibit the greatest SER (\* 1.2 ± 0.1), and NaErF<sub>4</sub> short-wave infrared (SWIR) probes achieve PLQY values approaching 12 % at 1,500-1,700 nm. Collectively, these findings support the

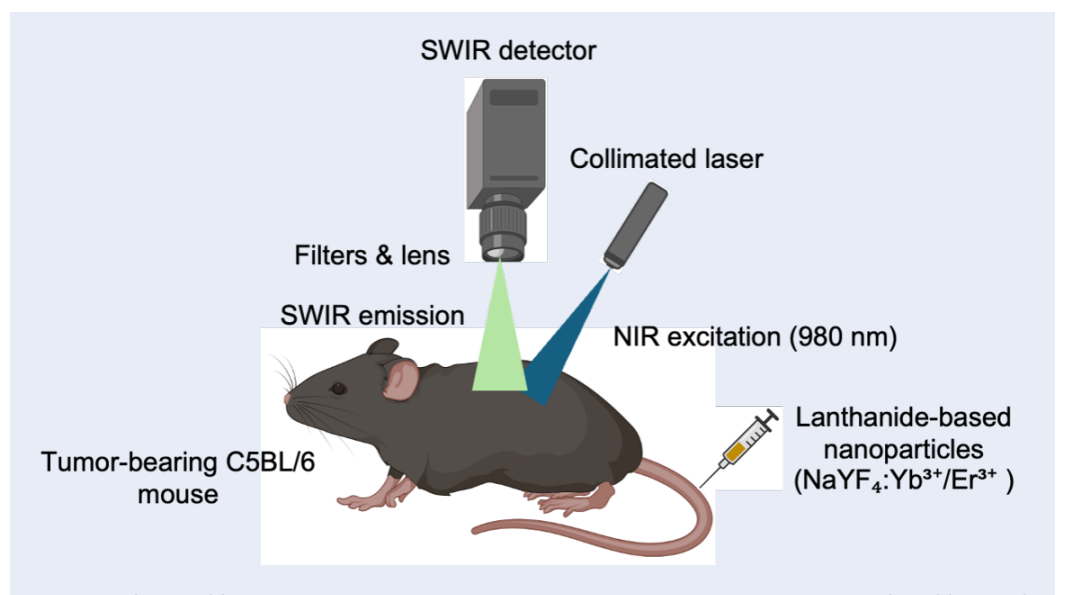
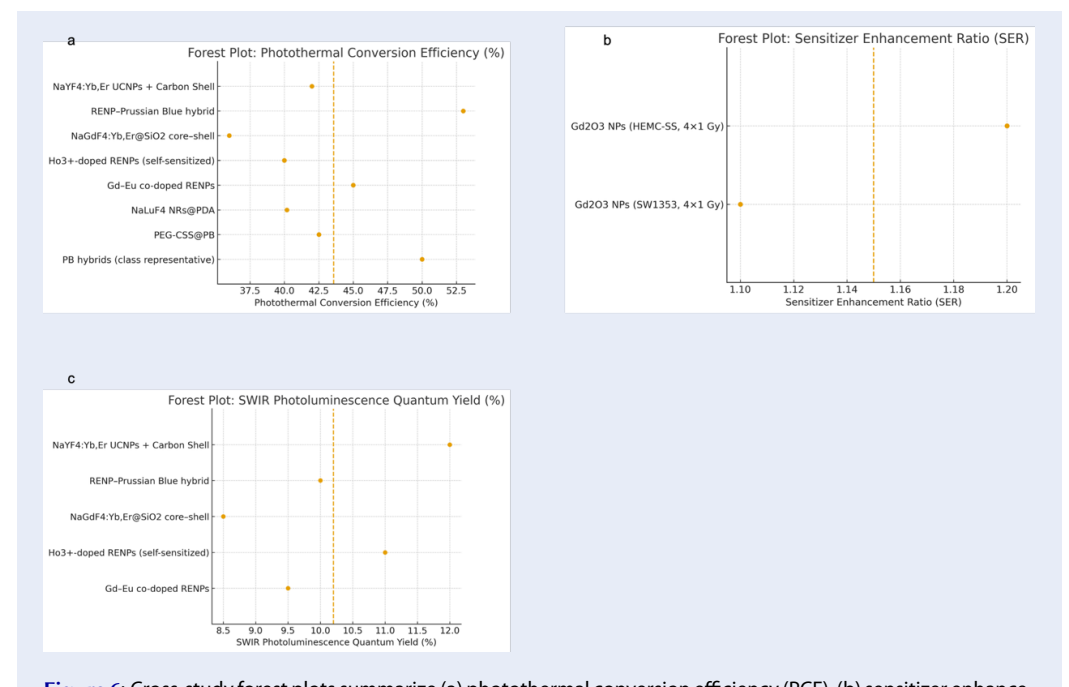


Figure 5: The portable SWIR-imaging prototype integrates an InGaAs camera (50 ms exposure), adjustable optical filter, and  $0.14~\mathrm{W~cm^{-2}}$  laser, enabling high-sensitivity imaging in a compact, versatile design for biomedical use.



**Figure 6**: Cross-study forest plots summarize (a) photothermal conversion efficiency (PCE), (b) sensitizer enhancement ratio (SER) of  $Gd_2O_3$  radiosensitizers under fractionated radiotherapy, and (c) SWIR photoluminescence quantum yield (PLQY). Dashed vertical lines represent pooled unweighted means due to inconsistent variance reporting across studies  $^{108,109}$ . **Note: PCE**, photothermal conversion efficiency; **SER**, sensitizer enhancement ratio; **SWIR**, short-wave infrared; **PLQY**, photoluminescence quantum yield; **Gd<sub>2</sub>O<sub>3</sub>**, gadolinium oxide.

- 1. Material QC & Standardization Harmonize PLQY, PCE, RT metrics
- 2. Optical & Radiotherapy Phantoms
   Validate SWIR penetration & dose enhancement
  - 3. Small-Animal Co-Registration
     Combine SWIR imaging with radiotherapy
- 4. GLP Toxicology & ISO 10993
   Systemic toxicity, biodistribution, immune response
  - 5. Indication Selection
     Focus on melanoma & superficial tumors

## 6. First-in-Human Feasibility - Early Phase 0/1 SWIR-guided PTT ± RT

**Figure 7**: The clinical translation roadmap for tri-modal lanthanide-based nanoparticles (LnNPs) progresses from material quality control and standardized performance metrics (PLQY, PCE, SER) to phantom validation, small-animal co-registration, GLP toxicology, ISO 10993 assays, and indication-specific trials for melanoma and superficial tumors. This framework highlights harmonized evaluation and regulatory readiness, distinguishing this review from earlier reports.

development of multifunctional core-shell architectures that couple Nd<sup>3+</sup>/Yb<sup>3+</sup> photothermal cores with Gd<sup>3+</sup>-enriched shells, thereby enabling simultaneous SWIR imaging and radiosensitization <sup>20,34</sup>.

# TOXICOLOGY AND BIODISTRIBUTION OF LANTHANIDE-BASED NANOPARTICLES

The biocompatibility and *in vivo* fate of lanthanide-doped nanoparticles (LnNPs) are pivotal for clinical translation. Recent research (2024–2025) indicates that toxicity, clearance, and organ retention depend strongly on particle size, coating, and delivery route. A meta-review of 120 preclinical datasets reported that PEG- or silica-coated upconversion nanoparticles show negligible cytotox-

icity below 100 μg mL<sup>-1</sup>, whereas uncoated fluoride cores trigger oxidative stress and lanthanideion leakage above 200  $\mu g\ mL^{-1},$  elevating ROS levels 111. Particle size governs clearance kineticsultrasmall LnNPs (< 5.5 nm) undergo rapid renal excretion  $(t_1/_2 \approx 2-4 \text{ h})$ , while larger (> 10 nm) ones are sequestered by the mononuclear phagocyte system (MPS), mainly in liver and spleen. ICP-MS and LA-ICP-MS analyses confirm biphasic elimination: a rapid plasma-clearance phase  $(t_1/2 \approx 6-12)$ h) and a slower organ-depot phase lasting up to 30 days. Gadolinium-based systems exhibit variable long-term retention; macrocyclic chelates such as Gd-DOTA are largely excreted, whereas linear or polymeric Gd complexes can persist in bone tissue beyond 60 days 112. Conversely, degradable or ultrasmall nanostructures such as NaGdF4@PEG (5 nm) and SiO2-encapsulated NaYF4:Yb,Er (4 nm) achieve >80% renal clearance within 48 h with minimal hepatic accumulation. PEGylation, zwitterionic, and biomimetic coatings reduce complement activation and immune uptake, improving systemic compatibility. Nonetheless, cumulative dosing and chronic exposure effects remain insufficiently characterized. Long-term toxicology studies ( $\geq$  90 days) assessing hematological, hepatic, and renal indices are urgently needed before first-in-human applications <sup>8</sup>. Future studies must adopt standardized frameworks for NOAEL, clearance half-life, and biodistribution (%ID g<sup>-1</sup>), ensuring compliance with ISO 10993-22 to facilitate regulatory translation <sup>36,113</sup>.

### **DISCUSSION**

Lanthanide-based nanoparticles (LnNPs) have rapidly become versatile theranostic platforms that integrate imaging and therapy. Their sharp emission bands, long-lived luminescence, and high atomic numbers render them well suited for short-wave infrared (SWIR) imaging, photothermal therapy (PTT), and radiosensitization 114-116. In PTT, LnNPs efficiently convert second-nearinfrared (NIR-II, 1,000-1,700 nm) light into localized heat; this deeper-penetrating wavelength reduces scattering and improves treatment precision. Nd<sup>3+</sup>- and Yb<sup>3+</sup>-doped nanoparticles demonstrate high photothermal conversion efficiencies (PCEs) with robust thermal stability and minimal photobleaching 114. As radiosensitizers, Gd3+ and Yb3+ ions enhance X-ray and γ-ray absorption, thereby increasing reactive oxygen species (ROS) formation and DNA damage while allowing lower radiation doses 115,117,118. For diagnostics, LnNPs provide superior SWIR imaging with deep-tissue penetration and negligible autofluorescence. Upand down-conversion processes enable multimodal fluorescence and photoacoustic imaging, facilitating precise tumour localization 119. tumour-responsive lanthanide platform has been shown to enhance dual-modal imaging resolution and therapeutic monitoring 120.

Hybrid constructs combining lanthanides with carbon, noble metals, or chalcogenides (e.g.,  $Cu_xS$ ,  $MoS_2$ ) produce efficient, biocompatible NIR-triggered hyperthermia <sup>121</sup>. Liu et al. <sup>122</sup> developed a heterojunction UCNP@NBOF-FePc-PFA nanostructure that unifies SWIR imaging, PTT, PDT, and radio-dynamic therapy (RDT) and achieves a PCE of 42.5 %. *In vivo*, synergistic X-ray and 730 nm laser treatments yielded superior tumour inhibition. NaErF<sub>4</sub> nanoparticles (1,525 nm emission) afforded high-contrast SWIR imaging <sup>122,123</sup>,

 $Ba_{1.4}Mn_{0.6}Lu_{0.5}Gd_{0.5}F_7:Yb^{3+}/Er^{3+}/Ho^{3+}$ while trimodal luminescence/MRI/CT readenabled outs<sup>81</sup>. Polydopamine-coated NaLuF<sub>4</sub> nanorods (NRs@PDA) displayed 40.18 % PCE for NIR-II imaging and PTT 124, and PEGylated core-shell-shell nanoparticles (PEG-CSS@PB) allowed effective real-time NIR-II-guided ablation 123. In RDT, Dy/Mn phosphate nanoparticles released Dy3+/Mn2+ in the acidic tumour microenvironment, thereby amplifying ROS, depleting GSH, and activating STING-mediated immune modulation 125, while Eu/Gd-doped ZnO improved X-ray-induced ROS generation and MRI/CT imaging 126. Motexafin gadolinium (MGd) additionally demonstrated dual radiosensitization and selective tumour inhibition 69. Pre-clinical results confirm that Gd-based nanoparticles attenuate tumour growth and prolong survival under fractionated X-ray RT, with standardized sensitizer metrics (SER, DMF, DEF) facilitating translation. Clinical trials such as Gd-NCT (NCT05313340) and AGuIX® report MRI-guided radiosensitization benefits in brain metastasis and hepatocellular carcinoma models 71,127-129. Quantitatively, LnNPs achieve PCEs of 40-53 % under NIR-II excitation: NaLuF<sub>4</sub> NRs@PDA (40.2 %), PEG-CSS@PB (42.5 %), and Prussian Blue hybrids (50 %) 130. Radiosensitization yields SER values of 1.1-1.2 with 4 × 1 Gy RT, extending survival (87 vs. 56 days for RT alone). Imaging beyond 1,100 nm produces superior SBR (3.3 vs. 1.4 at 520 nm), with NIR-IIb/I (1,500-1,900 nm) extended to 1,852-1,900 nm for ultra-highresolution vascular and intestinal imaging 124,131-133 (Table 5).

Although lanthanide nanoparticles (LnNPs) exhibit remarkable potential for cancer theranostics, their clinical translation remains limited by several challenges. The inherently low quantum yield of shortwave infrared (SWIR) imaging reduces sensitivity and spatial resolution; therefore, strategies such as optimized lanthanide doping (Yb<sup>3+</sup>, Er<sup>3+</sup>, Nd<sup>3+</sup>), surface modification, dye sensitization\*\*,\*\* and semiconductor hybridization have been implemented to improve quantum efficiency 139. The restricted tissue penetration of near-infrared (NIR) light further impairs photothermal therapy (PTT) for deepseated tumors, for which optical-fiber-assisted NIR-II delivery has shown promise <sup>140</sup>. Pharmacokinetic heterogeneity and non-specific biodistribution still present obstacles, frequently leading to incomplete tumor accumulation and off-target toxicity. Surface PEGylation and polymeric coatings can prolong circulation and attenuate immune clearance,

Table 5: Cross-study quantitative summary (PCE, SER/DMF/DEF, SWIR SNR)

S.No	Modal- ity	Metric	Representative System	Value (Conditions)	Model/ Notes	Ref.
1	PTT	PCE (%)	NaLuF <sub>4</sub> NRs@PDA (polydopamine-coated nanorods)	40.18% at 1064 nm; demonstrated in vivo tumor ablation	NIR-IIb guided photothermal therapy; deep tissue ablation efficiency validated in melanoma xenograft	124
2	PTT	PCE (%)	PEG-CSS@PB (Prussian Blue-coated NaErF <sub>4</sub> @NaYF <sub>4</sub> @NaNdF <sub>4</sub> core-shell-shell UCNPs)	≈42.5% at 730 nm excitation	Dual SWIR imaging and photothermal therapy; synergistic emission-absorption coupling	134
3	PTT	PCE (Class)	PB-based hybrid nanoplatforms (Fe-CN framework + LnNPs)	≈50% (808 nm, design- dependent)	Reported across multiple Prussian Blue-derived nanodesigns optimized for NIR absorption	131
4	RT	SER (fraction- ated)	Gd <sub>2</sub> O <sub>3</sub> nanoparticles	$SER_{4\times 1} Gy = 1.2$ (HEMC-SS); 1.1 (SW1353)	In-vitro radiotherapy (1 Gy $\times$ 4 fractions); Gd = 800 $\mu$ M	135
5	RT	Survival (in vivo)	Gd <sub>2</sub> O <sub>3</sub> NP + 4 Gy (single fraction)	87 d vs 56 d (IT+RT vs RT alone)	HEMC-SS xenograft; intratumoral (IT) dosing > intravenous (IV) route; prolonged tumor control	135
6	RT	DEF/DMF (method)	Gd-NPs in e-brachytherapy	Energy-resolved DEF & DMF; optimized Gd conc. at 50/70 kVp	Standardized X-ray phantom dosimetry model for localized Gd enhancement	132
7	SWIR	SBR (Signal- to- Background Ratio)	Vascular imaging > 1100 nm using NaErF <sub>4</sub> @NaLuF <sub>4</sub> UCNPs	SBR = 3.3 vs 1.4 (520 nm)/1.3 (720 nm)	Identical setup; improved vascular contrast at longer wavelength (> 1100 nm)	136
8	SWIR	Window exten- sion	NIR-II-L (1500–1900 nm) lanthanide nanoprobes	High-resolution multiplexed in vivo imaging in 1852–1900 nm	Demonstrated ultra-long wavelength bioimaging with minimal scattering	1334
9	Toxi- cology / Biodis- tribu- tion	Clear- ance t½ (h)	NaGdF₄@PEG (5 nm)	2–4 h (renal); > 80 % clearance within 48 h	Rapid renal excretion; minimal hepatic retention	137
10	Toxi- cology / Biodis- tribu- tion	Organ Reten- tion (days)	Linear vs Macrocyclic Gd-chelates	> 60 days (bone, linear) vs negligible (macrocyclic)	Heterogeneous long-term Gd deposition in bone tissue	138

Abbreviations: PCE, photothermal conversion efficiency; SER, sensitizer enhancement ratio; DMF, dose-modifying factor; DEF, dose-enhancement factor; SWIR, short-wave infrared; SBR, signal-to-background ratio; t½, half-life; %ID  $g^{-1}$ , percentage of injected dose per gram of tissue; NP, nanoparticle; Gd, gadolinium; NIR, near-infrared; IV, intravenous; IT, intratumoral.

yet active targeting strategies require further optimization 141. Long-term toxicity, biodegradability likewise warrant comprehensive evaluation prior to clinical adoption 111,142. In vivo tracking by laserablation inductively coupled plasma mass spectrometry (LA-ICP-MS) demonstrates that PEG-coated NaYF<sub>4</sub>-based upconverting nanoparticles (UCNPs) accumulate predominantly in the liver and spleen, exhibit minor distribution to the kidneys and heart, and remain sequestered within the mononuclear phagocyte system (MPS) unless the particles are ultrasmall or degradable. Gd-containing formulations pose specific risks of bone deposition, particularly when linear chelates are used, underscoring the need for chelate stability and dose control. Conversely, ultrasmall LnNPs (≤ 5.5 nm) permit efficient renal excretion, supporting the development of renal-clearable nanomedicines. Earlyphase AGuIX® (Gd-polysiloxane) clinical trials have demonstrated tumor selectivity, renal elimination and an acceptable safety profile, providing a translational precedent 143-146. Regulatory frameworks emphasize stringent safety assessment and material characterization: the U.S. Food and Drug Administration (FDA, 2022) requires complete chemistrymanufacturing-and-controls (CMC) data, particlesize characterization and risk-based toxicology; the European Union's REACH (2020) regulation mandates nanoform-specific dossiers and dispersionstability testing (OECD TG 318); and ISO/TR 10993-22 outlines biological evaluation of nanomaterials 37,147,148.

Future research should prioritize the development of stimuli-responsive lanthanide-doped nanoparticles (LnNPs) capable of controlled drug release and integrated imaging, while leveraging artificial intelligence-assisted image analytics and multimodal therapy. The synergistic combination of photothermal therapy (PTT), radiotherapy, and immunotherapy has the potential to overcome tumor heterogeneity and enhance therapeutic precision 149-151. Successful clinical translation will require the standardization of material parameters including dopant ratios, photoluminescence quantum yield (PLQY), photothermal conversion efficiency (PCE), and scintillation emission ratio (SER)and the validation of performance in optical and radiotherapy phantoms in accordance with ASTM/ISO protocols. Subsequent small-animal co-registration studies that integrate short-wave infrared (SWIR) imaging with real-time radiotherapy are needed to evaluate biodistribution, dosimetry, and efficacy. Comprehensive good laboratory practice (GLP) and ISO 10993 toxicology testing, systemic and immune profiling, and clearance studies are essential prerequisites for first-in-human trials. Early-phase feasibility studies should focus on optically accessible tumors, such as melanomas and head-and-neck cancers, employing SWIR-guided PTT or radiotherapy in Phase 0/1 trials <sup>20,152–154</sup>. Ultimately, interdisciplinary collaboration among materials scientists, oncologists, and regulatory experts will be critical for advancing LnNPs toward precision, multimodal, and patient-centered cancer care.

### **CONCLUSIONS**

Lanthanide-based nanoparticles (LnNPs) have emerged as versatile theranostic platforms that integrate photothermal therapy (PTT), radiosensitization, and short-wave infrared (SWIR) imaging, thereby enabling precise and efficient cancer treatment. Their unique optical and physicochemical properties enable deep-tissue imaging, targeted tumor accumulation, and real-time therapy mon-Under near-infrared (NIR) excitation, lanthanide-doped systems generate localized heat for PTT, serve as high-Z radiosensitizers that augment radiation energy deposition, and produce strong SWIR signals for treatment tracking. This multimodal synergy improves therapeutic efficacy while minimizing off-target effects relative to single-modality approaches. However, clinical translation will necessitate standardized synthesis, reliable surface functionalization for targeted delivery, and rigorous evaluation of biodistribution, dosimetry, and long-term biosafety. With harmonized performance benchmarks and translational frameworks, LnNP-based nanoplatforms are poised to become components of next-generation precision oncology and integrated treatment planning.

### **ABBREVIATIONS**

5-FU: 5-Fluorouracil; ADP: Adenosine Diphosphate; ATM: Ataxia Telangiectasia Mutated; ATR: Ataxia Telangiectasia and Rad3-Related; BALB: BALB/c mouse strain; BCS: Biopharmaceutics Classification System; CA: Cancer Atlas / Cancer Journal; CR: Complete Response; Cross-Relaxation; CT: Computed Tomography; DEF: Dose-Enhancement Factor; DMF: Dose-Modifying Factor; DNA: Deoxyribonucleic Acid; DOX: Doxorubicin; EBRT: External Beam Radiotherapy; EPR: Enhanced Permeability and Retention (effect); FDG: Fluorodeoxyglucose; FIH: First-in-Human; FIR: Fluorescence Intensity Ratio; Far Infrared; FWHM: Full Width at Half Maximum; GLP:

Good Laboratory Practice; GLOBOCAN: Global Cancer Observatory; GSH: Glutathione; HA: Hyaluronic Acid; ICP-MS: Inductively Coupled Plasma Mass Spectrometry; IGRT: Image-Guided Radiotherapy; IMRT: Intensity-Modulated Radiotherapy; LA-ICP-MS: Laser-Ablation Inductively Coupled Plasma Mass Spectrometry; LnNPs: Lanthanide-Doped Nanoparticles; MPS: Mononuclear Phagocyte System; MRI: Magnetic Resonance Imaging; MTT: 3-(4,5-Dimethylthiazol-2-yl)-2,5diphenyltetrazolium bromide assay; Nd3+-RENPs: Neodymium-doped Rare-Earth Nanoparticles; NIR: Near Infrared; NOAEL: No-Observed-Adverse-Effect L evel; O SA: O ptical S pectrum Analyzer; PARP: Poly (ADP-ribose) Polymerase; PB: Prussian Blue; PCE: Photothermal Conversion Efficiency; PDT: Photodynamic Therapy; PEG: Polyethylene Glycol; PL: Photoluminescence; PLQY: Photoluminescence Quantum Y ield; PS: Photosensitizers; PTA: Photothermal Agents; PTT: Photothermal Therapy; RDT: Radio-dynamic Therapy; RENP: Rare-Earth-Doped Nanoparticles; ROS: Reactive Oxygen Species; RT: Radiotherapy; SBR: Signal-to-Background Ratio; SER: Sensitizer Enhancement Ratio; SNR: Signal-to-Noise Ratio; STING: Stimulator of Interferon Genes; SWIR: Shortwave Infrared; UCNP: Upconversion Nanoparticles; UV: Ultraviolet; WDM: Wavelength Division Multiplexing

### **ACKNOWLEDGMENTS**

We express our gratitude to Dr. Irfan Aziz, Department of Pharmacy, Integral University, India for proofreading the article.

### **AUTHOR'S CONTRIBUTIONS**

All author contributed to the realization of this review. The first of the manuscript were written by Mohd Yaqub Khan and all authors commented on the successive versions of the manuscript. All authors have read and approved the final manuscript.

### **FUNDING**

None.

## AVAILABILITY OF DATA AND MATERIALS

Not applicable.

## ETHICS APPROVAL AND CONSENT TO PARTICIPATE

Not applicable.

### **CONSENT FOR PUBLICATION**

Not applicable.

### DECLARATION OF GENERATIVE AI AND AI-ASSISTED TECHNOLOGIES IN THE WRITING PROCESS

The authors declare that they have not used generative AI (a type of artificial intelligence technology that can produce various types of content including text, imagery, audio and synthetic data. Examples include ChatGPT, NovelAI, Jasper AI, Rytr AI, DALL-E, etc) and AI-assisted technologies in the writing process before submission.

### **COMPETING INTERESTS**

The authors declare that they have no competing interests.

### **NON-CITED REFERENCES**

References: 155, 156-159, 160-172

### REFERENCES

- Bray F, Ferlay J, Soerjomataram I, Siegel RL, Torre LA, Jemal A. Global cancer statistics 2018: GLOBOCAN estimates of incidence and mortality worldwide for 36 cancers in 185 countries. CA Cancer J Clin. 2018 Nov;68(6):394–424. PMID: 30207593. Available from: https://doi.org/10.3322/caac.21492.
- Sung H, Ferlay J, Siegel RL, Laversanne M, Soerjomataram I, Jemal A. Global Cancer Statistics 2020: GLOBOCAN Estimates of Incidence and Mortality Worldwide for 36 Cancers in 185 Countries. CA Cancer J Clin. 2021 May;71(3):209–249. PMID: 33538338. Available from: https://doi.org/10.3322/caac. 21660.
- Alvi MM, Nicoletto RE, Eshmawi BA, Kim HK, Cammarata CR, 3rd Ofner CM. Intracellular trafficking and cytotoxicity of a gelatine-doxorubicin conjugate in two breast cancer cell lines. J Drug Target. 2020 Jun;28(5):487–499. PMID: 31601131. Available from: https://doi.org/10.1080/1061186X. 2019.1679820.
- Diasio RB, Harris BE. Clinical pharmacology of 5-fluorouracil. Clin Pharmacokinet. 1989 Apr;16(4):215–237. PMID: 2656050. Available from: https://doi.org/10.2165/00003088-198916040-00002.
- Longley DB, Harkin DP, Johnston PG. 5-fluorouracil: mechanisms of action and clinical strategies. Nat Rev Cancer. 2003 May;3(5):330–338. PMID: 12724731. Available from: https://doi.org/10.1038/nrc1074.
- Baskar R, Lee KA, Yeo R, Yeoh KW. Cancer and radiation therapy: current advances and future directions. Int J Med Sci. 2012;9(3):193–199. PMID: 22408567. Available from: https: //doi.org/10.7150/ijms.3635.
- Delaney G, Jacob S, Featherstone C, Barton M. The role of radiotherapy in cancer treatment: estimating optimal utilization from a review of evidence-based clinical guidelines. Cancer. 2005 Sep;104(6):1129–1137. PMID: 16080176. Available from: https://doi.org/10.1002/cncr.21324.
- Verginadis II, Citrin DE, Ky B, Feigenberg SJ, Georgakilas AG, Hill-Kayser CE. Radiotherapy toxicities: mechanisms, management, and future directions. Lancet. 2025 Jan;405(10475):338–352. PMID: 39827884. Available from: https://doi.org/10.1016/S0140-6736(24)02319-5.

- Chen D, Parsa R, Chauhan K, Lukovic J, Han K, Taggar A. Review of brachytherapy clinical trials: a cross-sectional analysis of ClinicalTrials.gov. Radiat Oncol. 2024 Feb;19(1):22.
   PMID: 38351013. Available from: https://doi.org/10.1186/s13014-024-02415-8.
- Abdul Jalil R, Zhang Y. Biocompatibility of silica coated NaYF(4) upconversion fluorescent nanocrystals. Biomaterials. 2008 Oct;29(30):4122–4128. PMID: 18675453. Available from: https://doi.org/10.1016/j.biomaterials.2008.07.012.
- O'Connor JP, Aboagye EO, Adams JE, Aerts HJ, Barrington SF, Beer AJ. Imaging biomarker roadmap for cancer studies. Nat Rev Clin Oncol. 2017 Mar;14(3):169–186. PMID: 27725679. Available from: https://doi.org/10.1038/nrclinonc.2016.162.
- Hong G, Antaris AL, Dai H. Near-infrared fluorophores for biomedical imaging. Nat Biomed Eng. 2017;1(1):0010. Available from: https://doi.org/10.1038/s41551-016-0010.
- Park JY, Chang Y, Lee GH. Multi-modal imaging and cancer therapy using lanthanide oxide nanoparticles: current status and perspectives. Curr Med Chem. 2015;22(5):569– 581. PMID: 25439587. Available from: https://doi.org/10.2174/ 0929867322666141128162843.
- Chen G, Roy I, Yang C, Prasad PN. Nanochemistry and Nanomedicine for Nanoparticle-based Diagnostics and Therapy. Chem Rev. 2016 Mar;116(5):2826–2885. PMID: 26799741.
   Available from: https://doi.org/10.1021/acs.chemrev.5b00148.
- Xia Y, Yang R, Zhu J, Wang H, Li Y, Fan J. Engineered nanomaterials trigger abscopal effect in immunotherapy of metastatic cancers. Front Bioeng Biotechnol. 2022 Oct;10. PMID: 36394039. Available from: https://doi.org/10.3389/ fbioe.2022.890257.
- Zhong Y, Ma Z, Wang F, Wang X, Yang Y, Liu Y. In vivo molecular imaging for immunotherapy using ultra-bright near-infrared-llb rare-earth nanoparticles. Nat Biotechnol. 2019 Nov;37(11):1322–1331. PMID: 31570897. Available from: https://doi.org/10.1038/s41587-019-0262-4.
- Chen F, Goel S, Valdovinos HF, Luo H, Hernandez R, Barnhart TE. In Vivo Integrity and Biological Fate of Chelator-Free Zirconium-89-Labeled Mesoporous Silica Nanoparticles. ACS Nano. 2015 Aug;9(8):7950–7959. PMID: 26213260. Available from: https://doi.org/10.1021/acsnano.5b00526.
- Liu YQ, Qin LY, Li HJ, Wang YX, Zhang R, Shi JM. Application of lanthanide-doped upconversion nanoparticles for cancer treatment: a review. Nanomedicine (Lond). 2021
  Oct;16(24):2207–2242. PMID: 34533048. Available from: https://doi.org/10.2217/nnm-2021-0214.
- Huang L, Kakadiaris E, Vaneckova T, Huang K, Vaculovicova M, Han G. Designing next generation of photon upconversion: recent advances in organic triplet-triplet annihilation upconversion nanoparticles. Biomaterials. 2019 May;201:77–86. PMID: 30802685. Available from: https://doi.org/10.1016/j.biomaterials.2019.02.008.
- Yang M, Huang Y, Chen Z, Ye Q, Zeng Z, You X. Synthetic carbon-based lanthanide upconversion nanoparticles for enhanced photothermal therapy. Nat Commun. 2025 Jul;16(1):6343. PMID: 40634298. Available from: https://doi.org/10.1038/s41467-025-60454-5.
- Khan IA, Yu T, Yang M, Liu J, Chen Z. A Systematic Review of Toxicity, Biodistribution, and Biosafety in Upconversion Nanomaterials: Critical Insights into Toxicity Mitigation Strategies and Future Directions for Safe Applications. BME Front. 2025;6:0120. Available from: https://doi.org/10.34133/bmef.0120.
- Chen S, Han T, Tang BZ. Functional Polymeric Micromaterials Based on Aggregation-Induced Emission Luminogens. Adv Funct Mater. 2023;33(51):2307267. Available from: https://doi.org/10.1002/adfm.202307267.
- Page MJ, McKenzie JE, Bossuyt PM, Boutron I, Hoffmann TC, Mulrow CD. The PRISMA 2020 statement: an updated guideline for reporting systematic reviews. BMJ. 2021 Mar;372. PMID: 33782057. Available from: https://doi.org/10.1136/bmj. p.71
- 24. Haddaway NR, Page MJ, Pritchard CC, McGuinness LA.

- *PRISMA2020*: an R package and Shiny app for producing PRISMA 2020-compliant flow diagrams, with interactivity for optimised digital transparency and Open Synthesis. Campbell Syst Rev. 2022 Mar;18(2). PMID: 36911350. Available from: https://doi.org/10.1002/cl2.1230.
- Jiang X, Wang Y, Xu D, Lin B, Yang F, Lv R. Lanthanide-Based Nanocomposites for Photothermal Therapy under Near-Infrared Laser: Relationship between Light and Heat, Biostability, and Reaction Temperature. Langmuir. 2020 Apr;36(15):4033–4043. PMID: 32188251. Available from: https://doi.org/10.1021/acs.langmuir.0c00343.
- Zhao L, Zhang X, Wang X, Guan X, Zhang W, Ma J. Recent advances in selective photothermal therapy of tumor.
   J Nanobiotechnology. 2021 Oct;19(1):335. PMID: 34689765.
   Available from: https://doi.org/10.1186/s12951-021-01080-3.
- Salimi M, Mosca S, Gardner B, Palombo F, Matousek P, Stone N. Nanoparticle-Mediated Photothermal Therapy Limitation in Clinical Applications Regarding Pain Management. Nanomaterials (Basel). 2022;12(6). Available from: https://doi.org/ 10.3390/nano12060922.
- Zhang Y, Zhu X, Zhang J, Wu Y, Liu J, Zhang Y. Syner-gistic upconversion photodynamic and photothermal therapy under cold near-infrared excitation. J Colloid Interface Sci. 2021 Oct;600:513–529. PMID: 34034118. Available from: https://doi.org/10.1016/j.jcis.2021.05.017.
- Cui X, Ruan Q, Zhuo X, Xia X, Hu J, Fu R. Photothermal Nanomaterials: A Powerful Light-to-Heat Converter. Chem Rev. 2023 Jun;123(11):6891–6952. PMID: 37133878. Available from: https://doi.org/10.1021/acs.chemrev.3c00159.
- Cai Y, Chai T, Nguyen W, Liu J, Xiao E, Ran X. Phototherapy in cancer treatment: strategies and challenges. Signal Transduct Target Ther. 2025 Apr;10(1):115. PMID: 40169560. Available from: https://doi.org/10.1038/s41392-025-02140-y.
- Xie B, Xiao Z, Ling J, Peng Y, Chen T. Exploring the application of metal-based photothermal agents in photothermal therapy combined with immune checkpoint therapy. Front Pharmacol. 2025 Feb;16:1553158. PMID: 40017598. Available from: https://doi.org/10.3389/fphar.2025.1553158.
- Shi X, Tian Y, Liu Y, Xiong Z, Zhai S, Chu S, et al. Research Progress of Photothermal Nanomaterials in Multimodal Tumor Therapy. Front Oncol. 2022;12:939365. Available from: https://doi.org/10.3389/fonc.2022.939365.
- Kim S, Park Y, Han J, Kim H, Jang H, Kim S. Near-infrared long lifetime upconversion nanoparticles for ultrasensitive microRNA detection via time-gated luminescence resonance energy transfer. Nat Commun. 2025 Aug;16(1):7557. PMID: 40813766. Available from: https://doi.org/10.1038/s41467-025-62802-x.
- Ghorpade KB, Kumar M, Tiwari S. A review on composites based on upconversion nanoparticles and graphene oxide: development and theranostic applications centered at solid tumors. J Mater Sci Mater Des. 2024;19(1):48. Available from: https://doi.org/10.1186/s40712-024-00187-3.
- Jiang C, Chen Y, Li X, Li Y. An intelligent NIR-IIb-responsive lanthanide@metal-organic framework core-shell nanocatalyst for combined deep-tumor therapy. J Mater Chem B. 2024 Sep;12(35):8626–8632. PMID: 39189804. Available from: https://doi.org/10.1039/D4TB01321B.
- Mirmajidi H, Lee H, Nipu N, Thomas J, Gajdosechova Z, Kennedy D. Nano-bio interactions of Gum Arabic-stabilized lanthanide-based upconverting nanoparticles: in vitro and in vivo study. J Mater Chem B. 2024 Dec;13(1):160–176. PMID: 39539248. Available from: https://doi.org/10.1039/ D4TB01579G.
- Du P, Wei Y, Liang Y, An R, Liu S, Lei P. Near-Infrared-Responsive Rare Earth Nanoparticles for Optical Imaging and Wireless Phototherapy. Adv Sci (Weinh). 2024 Feb;11(8).
   PMID: 37946706. Available from: https://doi.org/10.1002/advs.202305308.
- 38. Gao T, Gao S, Li Y, Zhang R, Dong H. The Down-Shifting Luminescence of Rare-Earth Nanoparticles for Multimodal

- Imaging and Photothermal Therapy of Breast Cancer. Biology (Basel). 2024;13(3). Available from: https://doi.org/10.3390/biology13030156.
- Wang S, Zhang C, Fang F, Fan Y, Yang J, Zhang J. Beyond traditional light: NIR-II light-activated photosensitizers for cancer therapy. J Mater Chem B. 2023 Sep;11(35):8315–8326. PMID: 37523205. Available from: https://doi.org/10.1039/D3TB00668A.
- Wang X, Li H, Li F, Han X, Chen G. Prussian blue-coated lanthanide-doped core/shell/shell nanocrystals for NIR-II image-guided photothermal therapy. Nanoscale. 2019 Nov;11(45):22079–22088. PMID: 31720650. Available from: https://doi.org/10.1039/C9NR07973D.
- Kang D, Jeon E, Kim S, Lee J. Lanthanide-Doped Upconversion Nanomaterials: Recent Advances and Applications. Biochip J. 2020;14(1):124–135. PMID: 32218896. Available from: https://doi.org/10.1007/s13206-020-4111-9.
- 42. Chen G, Qiu H, Prasad PN, Chen X. Upconversion nanoparticles: design, nanochemistry, and applications in theranostics. Chem Rev. 2014 May;114(10):5161–5214. PMID: 24605868. Available from: https://doi.org/10.1021/cr400425h.
- Meng M, Zhang T, Wang J, Cheng Z, Liu Y, Qiao X. NaYF4:Yb3+/Tm3+@NaYF4:Yb3+ Upconversion Nanoparticles for Optical Temperature Monitoring and Self-Heating in Photothermal Therapy. ACS Appl Nano Mater. 2022;6(1):759–771. Available from: https://doi.org/10.1021/acsanm.2c05110.
- Yang W, Hicks DR, Ghosh A, Schwartze TA, Conventry B, Goreshnik I. Design of high-affinity binders to immune modulating receptors for cancer immunotherapy. Nat Commun. 2025 Feb;16(1):2001. PMID: 40011465. Available from: https://doi.org/10.1038/s41467-025-57192-z.
- Wu T, Zhang X, Cai S, Zhang W, Yang R. Prussian blue nanocages as efficient radical scavengers and photothermal agents for reducing amyloid-beta induced neurotoxicity. Colloids Surf B Biointerfaces. 2025 Feb;246:114369. PMID: 39536606. Available from: https://doi.org/10.1016/j.colsurfb. 2024.114369.
- Baziulyte-Paulaviciene D, Karabanovas V, Stasys M, Jarockyte G, Poderys V, Sakirzanovas S. Synthesis and functionalization of NaGdF4:Yb,Er@NaGdF4 core-shell nanoparticles for possible application as multimodal contrast agents. Beilstein J Nanotechnol. 2017 Sep;8:1815–1824. PMID: 28904843. Available from: https://doi.org/10.3762/bjnano.8.183.
- Rakesh Arul ZJ, Li X, Bell FM, Tew A, Ducati C, Rao A, et al. Efficient short-wave infrared upconversion by self-sensitized holmium-doped nanoparticles. arXiv. 2024;11. Available from: https://doi.org/10.48550/arXiv.2411.19949.
- 48. Wang GD, Chen H, Tang W, Lee D, Xie J. Gd and Eu Co-Doped Nanoscale Metal-Organic Framework as a T1-T2 Dual-Modal Contrast Agent for Magnetic Resonance Imaging. Tomography. 2016 Sep;2(3):179–187. PMID: 30042963. Available from: https://doi.org/10.18383/j.tom.2016.00226.
- Li Z, Gong J, Lu S, Li X, Gu X, Xu J. Photothermal lanthanide nanomaterials: from fundamentals to theranostic applications. BMEmat. 2024;2(4). Available from: https://doi.org/ 10.1002/bmm2.12088.
- Fan Q, Sun C, Hu B, Wang Q. Recent advances of lanthanide nanomaterials in Tumor NIR fluorescence detection and treatment. Mater Today Bio. 2023 May;20:100646. PMID: 37214552. Available from: https://doi.org/10.1016/j.mtbio. 2023.100646.
- Kang D, Kim HS, Han S, Lee Y, Kim YP, Lee DY. A local water molecular-heating strategy for near-infrared long-lifetime imaging-guided photothermal therapy of glioblastoma. Nat Commun. 2023 May;14(1):2755. PMID: 37179387. Available from: https://doi.org/10.1038/s41467-023-38451-3.
- Shi X, Cao C, Zhang Z, Tian J, Hu Z. Radiopharmaceutical and Eu3+ doped gadolinium oxide nanoparticles mediated triple-excited fluorescence imaging and image-guided surgery. J Nanobiotechnology. 2021 Jul;19(1):212. PMID: 34271928. Available from: https://doi.org/10.1186/s12951-021-00920-6.

- Tegafaw T, Zhao D, Liu Y, Yue H, Saidi AK, Baek A. High Quantum Yields and Biomedical Fluorescent Imaging Applications of Photosensitized Trivalent Lanthanide Ion-Based Nanoparticles. Int J Mol Sci. 2024 Oct;25(21):11419.
   PMID: 39518971. Available from: https://doi.org/10.3390/ iims252111419.
- Parchur AK, Li Q, Zhou A. Near-infrared photothermal therapy of Prussian-blue-functionalized lanthanide-ion-doped inorganic/plasmonic multifunctional nanostructures for the selective targeting of HER2-expressing breast cancer cells. Biomater Sci. 2016 Nov;4(12):1781–1791. PMID: 27768147. Available from: https://doi.org/10.1039/C6BM00306K.
- Wang M, Li B, Du Y, Bu H, Tang Y, Huang Q. Fluorescence imaging-guided cancer photothermal therapy using polydopamine and graphene quantum dot-capped Prussian blue nanocubes. RSC Adv. 2021 Feb;11(15):8420–8429.
   PMID: 35423381. Available from: https://doi.org/10.1039/D0RA10491D.
- Gao X, Wang Q, Cheng C, Lin S, Lin T, Liu C. The Application of Prussian Blue Nanoparticles in Tumor Diagnosis and Treatment. Sensors (Basel). 2020 Dec;20(23):6905. PMID: 33287186. Available from: https://doi.org/10.3390/s20236905.
- 57. Luo H, Gao S. Recent advances in fluorescence imaging-guided photothermal therapy and photodynamic therapy for cancer: from near-infrared-I to near-infrared-II. J Control Release. 2023 Oct;362:425–445. PMID: 37660989. Available from: https://doi.org/10.1016/j.jconrel.2023.08.056.
- Piotrowski W, Trejgis K, Maciejewska K, Ledwa K, Fond B, Marciniak L. Thermochromic Luminescent Nanomaterials Based on Mn4+/Tb3+ Codoping for Temperature Imaging with Digital Cameras. ACS Appl Mater Interfaces. 2020 Sep;12(39):44039–44048. PMID: 32902945. Available from: https://doi.org/10.1021/acsami.0c11730.
- Savchuk O, Carvajal Marti JJ, Cascales C, Haro-Gonzalez P, Sanz-Rodríguez F, Aguilo M. Bifunctional Tm3+,Yb3+:GdVO4@SiO2 Core-Shell Nanoparticles in HeLa Cells: Upconversion Luminescence Nanothermometry in the First Biological Window and Biolabelling in the Visible. Nanomaterials (Basel). 2020 May;10(5):993. PMID: 32455825. Available from: https://doi.org/10.3390/nano10050993.
- Du P, Wan X, Luo L, Li W, Li L. Thermally Stable Tb3+/Eu3+-Codoped K0.3Bi0.7F2.4 Nanoparticles with Multicolor Luminescence for White-Light-Emitting Diodes. ACS Appl Nano Mater. 2021;4(7):7062-7071. Available from: https://doi.org/ 10.1021/acsanm.1c01072.
- 61. Yang CC, Wang WY, Lin FH, Hou CH. Rare-Earth-Doped Calcium Carbonate Exposed to X-ray Irradiation to Induce Reactive Oxygen Species for Tumor Treatment. Int J Mol Sci. 2019 Mar;20(5):1148. PMID: 30845750. Available from: https://doi.org/10.3390/ijms20051148.
- Kaščáková S, Giuliani A, Lacerda S, Pallier A, Mercère P, Tóth
   X-ray-induced radiophotodynamic therapy (RPDT) using lanthanide micelles: beyond depth limitations. Nano Res. 2015;8(7):2373–2379. Available from: https://doi.org/10.1007/s12274-015-0747-5.
- Jin J, Zhao Q. Engineering nanoparticles to reprogram radiotherapy and immunotherapy: recent advances and future challenges. J Nanobiotechnology. 2020 May;18(1):75. PMID: 32408880. Available from: https://doi.org/10.1186/s12951-020-00629-y.
- Krzyszczyk P, Acevedo A, Davidoff EJ, Timmins LM, Marrero-Berrios I, Patel M. The growing role of precision and personalized medicine for cancer treatment. Technology (Singap). 2018;6(3-4):79–100. [Singap World Sci]. PMID: 30713991. Available from: https://doi.org/10.1142/S2339547818300020.
- Franzone P, Fiorentino A, Barra S, Cante D, Masini L, Cazzulo E. Image-guided radiation therapy (IGRT): practical recommendations of Italian Association of Radiation Oncology (AIRO). Radiol Med. 2016 Dec;121(12):958–965. PMID: 27601141. Available from: https://doi.org/10.1007/s11547-016-0674-x.

- Gong L, Zhang Y, Liu C, Zhang M, Han S. Application of Radiosensitizers in Cancer Radiotherapy. Int J Nanomedicine. 2021 Feb;16:1083–1102. PMID: 33603370. Available from: https://doi.org/10.2147/IJN.S290438.
- Fowler JF, Adams GE, Denekamp J. Radiosensitizers of hypoxic cells in solid tumors. Cancer Treat Rev. 1976 Dec;3(4):227–256. PMID: 1016978. Available from: https://doi.org/10.1016/S0305-7372(76)80012-6.
- Matsudaira H, Ueno AM, Furuno I. Iodine contrast medium sensitizes cultured mammalian cells to X rays but not to gamma rays. Radiat Res. 1980 Oct;84(1):144–148. PMID: 7454977. Available from: https://doi.org/10.2307/3575225.
- Liu Y, Zhang P, Li F, Jin X, Li J, Chen W. Metal-based NanoEnhancers for Future Radiotherapy: Radiosensitizing and Synergistic Effects on Tumor Cells. Theranostics. 2018 Feb;8(7):1824–1849. PMID: 29556359. Available from: https://doi.org/10.7150/thno.22172.
- Etheridge ML, Campbell SA, Erdman AG, Haynes CL, Wolf SM, McCullough J. The big picture on nanomedicine: the state of investigational and approved nanomedicine products. Nanomedicine. 2013 Jan;9(1):1–14. PMID: 22684017. Available from: https://doi.org/10.1016/j.nano.2012.05.013.
- Yu B, Lu X, Feng X, Zhao T, Li J, Lu Y. Gadolinium Oxide Nanoparticles Reinforce the Fractionated Radiotherapy-Induced Immune Response in Tri-Negative Breast Cancer via cGAS-STING Pathway. Int J Nanomedicine. 2023 Dec;18:7713–7728. PMID: 38115988. Available from: https://doi.org/10.2147/JJN.S428044.
- Muradova Z, Tannous D, Mostefa-Kara A, Cao-Pham TT, Lamy C, Broutin S. Gadolinium-based nanoparticles AGulX and their combination with ionizing radiation trigger AMPK-dependent proinflammatory reprogramming of tumor-associated macrophages. bioRxiv. 2024;.
- Ying X, Chen Q, Yang Y, Wu Z, Zeng W, Miao C. Nanomedicines harnessing cGAS-STING pathway: sparking immune revitalization to transform 'cold' tumors into 'hot' tumors. Mol Cancer. 2024 Dec;23(1):277. PMID: 39710707. Available from: https://doi.org/10.1186/s12943-024-02186-6.
- 74. Tillement O, Le Duc G, Roux S, Mowat P, Lux F, Janier M, et al. High efficiency radiosensitization with Sub-5 nm theranostic lanthanide-based nanoparticles. 2018:.
- Wu C, Cai R, Zhao T, Wu L, Zhang L, Jin J. Hyaluronic Acid-Functionalized Gadolinium Oxide Nanoparticles for Magnetic Resonance Imaging-Guided Radiotherapy of Tumors. Nanoscale Res Lett. 2020 Apr;15(1):94. PMID: 32335719. Available from: https://doi.org/10.1186/s11671-020-03318-9.
- Seo SJ, Han SM, Cho JH, Hyodo K, Zaboronok A, You H. Enhanced production of reactive oxygen species by gadolinium oxide nanoparticles under core-inner-shell excitation by proton or monochromatic X-ray irradiation: implication of the contribution from the interatomic de-excitation-mediated nanoradiator effect to dose enhancement. Radiat Environ Biophys. 2015 Nov;54(4):423–431. PMID: 26242374. Available from: https://doi.org/10.1007/s00411-015-0612-7.
- Zhu X, Qiu CJ, Cao JJ, Duosiken D, Zhang Y, Pei BG. Radiosensitization of Rare-Earth Nanoparticles Based on the Consistency Between Its K-Edge and the X-Ray Bremsstrahlung Peak. J Funct Biomater. 2025 Jan;16(2):41. PMID: 39997575. Available from: https://doi.org/10.3390/jfb16020041.
- Li Y, Qi Y, Zhang H, Xia Z, Xie T, Li W. Gramscale synthesis of highly biocompatible and intravenous injectable hafnium oxide nanocrystal with enhanced radiotherapy efficacy for cancer theranostic. Biomaterials. 2020 Jan;226:119538. PMID: 31639541. Available from: https://doi.org/10.1016/j.biomaterials.2019.119538.
- Kuang Y, Zhang Y, Zhao Y, Cao Y, Zhang Y, Chong Y. Dual-Stimuli-Responsive Multifunctional Gd2Hf2O7 Nanoparticles for MRI-Guided Combined Chemo-/Photothermal-/Radiotherapy of Resistant Tumors. ACS Appl Mater Interfaces. 2020 Aug;12(32):35928–35939. PMID: 32686939. Available from: https://doi.org/10.1021/acsami.0c09422.

- Sherstiuk AA, Tsymbal SA, Fakhardo AF, Morozov VN, Krivoshapkina EF, Hey-Hawkins E. Hafnium Oxide-Based Nanoplatform for Combined Chemoradiotherapy. ACS Biomater Sci Eng. 2021 Dec;7(12):5633– 5641. PMID: 34714630. Available from: https: //doi.org/10.1021/acsbiomaterials.1e00973.
- Teo RD, Termini J, Gray HB. Lanthanides: Applications in Cancer Diagnosis and Therapy. J Med Chem. 2016 Jul;59(13):6012–6024. PMID: 26862866. Available from: https://doi.org/10.1021/acs.jmedchem.5b01975.
- Xu Z, Luo T, Mao J, McCleary C, Yuan E, Lin W. Monte Carlo Simulation-Guided Design of a Thorium-Based Metal-Organic Framework for Efficient Radiotherapy-Radiodynamic Therapy. Angew Chem Int Ed Engl. 2022 Nov;61(46). PMID: 36149753. Available from: https://doi.org/10.1002/anie.202208685.
- Ni K, Lan G, Lin W. Nanoscale Metal-Organic Frameworks Generate Reactive Oxygen Species for Cancer Therapy. ACS Cent Sci. 2020 Jun;6(6):861–868. PMID: 32607433. Available from: https://doi.org/10.1021/acscentsci.0c00397.
- Mane SN, Kolekar SK, Sapnar KB, Dhole SD. Gamma radiation induced modification in metal-organic framework: a case study. J Radioanal Nucl Chem. 2024;333(6):3115–3122.
   Available from: https://doi.org/10.1007/s10967-024-09430-9.
- Ndabankulu VO, Maddila S, Jonnalagadda SB. Synthesis of Lanthanide Doped TiO2 Nanoparticles and Their Photocatalytic Activity under Visible Light. Can J Chem. 2019;97(9):672–681. Available from: https://doi.org/10.1139/ cjc-2018-0408.
- Chen Y, Li N, Wang J, Zhang X, Pan W, Yu L. Enhancement of mitochondrial ROS accumulation and radiotherapeutic efficacy using a Gd-doped titania nanosensitizer. Theranostics. 2019 Jan;9(1):167–178. PMID: 30662560. Available from: https://doi.org/10.7150/thno.28033.
- Jang H, Choi MH, Yim Y, Kim YK, Min DH. Dual-Wavelength Irradiation and Dox Delivery for Cancer Cell Ablation with Photocatalytic Pr Doped TiO2/NGO Hybrid Nanocomposite. Adv Healthc Mater. 2015 Aug;4(12):1833–1840. PMID: 26085286. Available from: https://doi.org/10.1002/adhm. 201500157
- Li H, Liu H, Wong KL, All AH. Lanthanide-doped upconversion nanoparticles as nanoprobes for bioimaging. Biomater Sci. 2024 Sep;12(18):4650–4663. PMID: 39150405. Available from: https://doi.org/10.1039/D4BM00774C.
- Malhotra K, Hrovat D, Kumar B, Qu G, Houten VJ, Ahmed R. Lanthanide-Doped Upconversion Nanoparticles: Exploring A Treasure Trove of NIR-Mediated Emerging Applications. ACS Appl Mater Interfaces. 2023 Jan;15(2):2499–2528. PMID: 36602515. Available from: https://doi.org/10.1021/acsami. 2c12370.
- Li P, Yan Y, Chen B, Zhang P, Wang S, Zhou J. Lanthanide-doped upconversion nanoparticles complexed with nano-oxide graphene used for upconversion fluorescence imaging and photothermal therapy. Biomater Sci. 2018 Mar;6(4):877–884. PMID: 29493665. Available from: https://doi.org/10.1039/C7BM011131.
- Wei HL, Zheng W, Zhang X, Suo H, Chen B, Wang Y. Tuning Near-Infrared-to-Ultraviolet Upconversion in Lanthanide-Doped Nanoparticles for Biomedical Applications. Adv Opt Mater. 2023;11(11). Available from: https://doi.org/10.1002/ adom.202201716.
- Naczynski DJ, Sun C, Türkcan S, Jenkins C, Koh AL, Ikeda D. X-ray-induced shortwave infrared biomedical imaging using rare-earth nanoprobes. Nano Lett. 2015 Jan;15(1):96–102. PMID: 25485705. Available from: https://doi.org/10.1021/nl504123r.
- Byrd BK, Folaron MR, Leonor JP, Strawbridge RR, Cao X, Bruza P. Characterizing short-wave infrared fluorescence of conventional near-infrared fluorophores. J Biomed Opt. 2019 Mar;24(3):1–5. PMID: 30851014. Available from: https://doi.org/10.1117/1.JBO.24.3.035004.

- Wang R, Zhang F. NIR luminescent nanomaterials for biomedical imaging. J Mater Chem B. 2014 May;2(17):2422– 2443. PMID: 32261412. Available from: https://doi.org/10. 1030/c/3tb21447h
- Rogach AL, Eychmüller A, Hickey SG, Kershaw SV. Infraredemitting colloidal nanocrystals: synthesis, assembly, spectroscopy, and applications. Small. 2007 Apr;3(4):536–557.
   PMID: 17340666. Available from: https://doi.org/10.1002/smll. 200600625.
- Naczynski DJ, Stafford JH, Türkcan S, Jenkins C, Koh AL, Sun C. Rare-earth-doped nanoparticles for short-wave infrared fluorescence bioimaging and molecular targeting of alphaVbeta3-expressing tumors. Mol Imaging. 2018;17. PMID: 30246593. Available from: https://doi.org/10.1177/ 1536012118799131.
- Wang Z, Zhang T, Pi L, Xiang H, Dong P, Lu C. Large-scale one-pot synthesis of water-soluble and biocompatible upconversion nanoparticles for dual-modal imaging. Colloids Surf B Biointerfaces. 2020;p. 111480. PMID: 33250414. Available from: https://doi.org/10.1016/j.colsurfb.2020.111480.
- Veggel JW. Near-infrared Emission of Redispersible Er3+, Nd3+, and Ho3+ Doped LaF3 Nanoparticles. Nano Lett. 2002;2(7):733-737. Available from: https://doi.org/10.1021/ nl025562a.
- Wang F, Zhang Y, Fan X, Wang M. Facile synthesis of water-soluble LaF3:Ln3+ nanocrystals. J Mater Chem. 2006;16(11):1031. Available from: https://doi.org/10.1039/b518262i.
- Li M, Hao ZH, Peng XN, Li JB, Yu XF, Wang QQ. Controllable energy transfer in fluorescence upconversion of NdF3 and NaNdF4 nanocrystals. Opt Express. 2010;18(4):3364. Available from: https://doi.org/10.1364/OE.18.003364.
- 101. Chen G, Liu S, Law WC, Wu F, Swihart MT, Ågren H, et al. Core/Shell NaGdF4:Nd3+/NaGdF4 Nanocrystals with Efficient Near-Infrared to Near-Infrared Downconversion Photoluminescence for Bioimaging Applications. ACS Nano. 2012;6(4):2969–2977. PMID: 22401578. Available from: https://doi.org/10.1021/nn2042362.
- 102. Kamimura M, Saito Y, Soga K, Nagasaki Y. Preparation of PEG and Protein Co-immobilized Upconversion Nanophosphors as Near-infrared Biolabeling Materials. J Photopolym Sci Technol. 2008;21(2):183–187. Available from: https://doi. org/10.2494/photopolymer.21.183.
- Naczynski DJ, Tan MC, Zevon M, Wall B, Kohl J, Kulesa A. Rare-earth-doped biological composites as in vivo shortwave infrared reporters. Nat Commun. 2013;4(1):2199.
   PMID: 23873342. Available from: https://doi.org/10.1038/ ncomms3199.
- Zhao H, Xiao H, Liu Y, Ju H. Lanthanide-doped rare earth nanoparticles for near-infrared-II imaging and cancer therapy. BMEmat. 2023;1(3). Available from: https://doi.org/10. 1002/bmm2.12032.
- 105. Ren F, Wang F, Baghdasaryan A, Li Y, Liu H, Hsu R. Shortwave-infrared-light-emitting probes for the in vivo tracking of cancer vaccines and the elicited immune responses. Nat Biomed Eng. 2024 Jun;8(6):726–739. PMID: 37620621. Available from: https://doi.org/10.1038/s41551-023-01083-5.
- 106. Simon AA, Haye L, Alhalabi A, Gresil Q. Muñoz BM, Mornet S. Expanding the Palette of SWIR Emitting Nanoparticles Based on Au Nanoclusters for Single-Particle Tracking Microscopy. Adv Sci (Weinh). 2024 Jun;11(24). PMID: 38639398. Available from: https://doi.org/10.1002/advs.202309267.
- Meng J, Cui Y, Wang Y. Rare Earth-Doped Nanoparticles for Near-Infrared II Image-Guided Photodynamic Therapy. ACS Appl Nano Mater. 2024;7(9):11008–11018. Available from: https://doi.org/10.1021/acsanm.4c02176.
- Du P, Wei Y, Liang Y, An R, Liu S, Lei P. Near-Infrared-Responsive Rare Earth Nanoparticles for Optical Imaging and Wireless Phototherapy. Adv Sci (Weinh). 2024 Feb;11(8).
   PMID: 37946706. Available from: https://doi.org/10.1002/advs.202305308.

- Li H, Liu H, Wong KL, All AH. Lanthanide-doped upconversion nanoparticles as nanoprobes for bioimaging. Biomater Sci. 2024 Sep;12(18):4650–4663. PMID: 39150405. Available from: https://doi.org/10.1039/D4BM00774C.
- Cui X, Ruan Q, Zhuo X, Xia X, Hu J, Fu R. Photothermal Nanomaterials: A Powerful Light-to-Heat Converter. Chem Rev. 2023 Jun;123(11):6891–6952. PMID: 37133878. Available from: https://doi.org/10.1021/acs.chemrev.3c00159.
- 111. Machova Urdzikova L, Mareková D, Vasylyshyn T, Matouš P, Patsula V, Oleksa V, et al. Toxicity of Large and Small Surface-Engineered Upconverting Nanoparticles for In Vitro and In Vivo Bioapplications. Int J Mol Sci. 2024;25. Available from: https://doi.org/10.3390/ijms25105294.
- 112. Chen K, Sun X, Liu Y, Li S, Meng D. Advances in clinical applications of microneedle. Front Pharmacol. 2025 Jun;16:1607210. PMID: 40641999. Available from: https://doi.org/10.3389/fphar.2025.1607210.
- 113. Feng X, Shang Y, Zhang H, Li R, Wang W, Zhang D. Enhanced luminescence and tunable magnetic properties of lanthanide coordination polymers based on fluorine substitution and phenanthroline ligand. RSC Adv. 2019 May;9(29):16328–16338. PMID: 35516386. Available from: https://doi.org/10.1039/C9RA01574D.
- 114. Zhang Y, Zhang S, Zhang Z, Ji L, Zhang J, Wang Q. Recent Progress on NIR-II Photothermal Therapy. Front Chem. 2021 Jul;9. PMID: 34395388. Available from: https://doi.org/10. 3389/fchem.2021.728066.
- 115. Choi J, Kim G, Cho SB, Im HJ. Radiosensitizing high-Z metal nanoparticles for enhanced radiotherapy of glioblastoma multiforme. J Nanobiotechnology. 2020 Sep;18(1):122. PMID: 32883290. Available from: https://doi.org/10.1186/s12951-020-00684-5.
- 116. Ferro-Flores G, Ancira-Cortez A, Ocampo-García B, Meléndez-Alafort L. Molecularly Targeted Lanthanide Nanoparticles for Cancer Theranostic Applications. Nanomaterials (Basel). 2024 Jan;14(3):296. PMID: 38334567. Available from: https://doi.org/10.3390/nano14030296.
- 117. Zhu X, Qiu CJ, Cao JJ, Duosiken D, Zhang Y, Pei BG. Radiosensitization of Rare-Earth Nanoparticles Based on the Consistency Between Its K-Edge and the X-Ray Bremsstrahlung Peak. J Funct Biomater. 2025 Jan;16(2):41. PMID: 39997575. Available from: https://doi.org/10.3390/jfb16020041.
- 118. Nosrati H, Salehiabar M, Charmi J, Yaray K, Ghaffarlou M, Balcioglu E. Enhanced In Vivo Radiotherapy of Breast Cancer Using Gadolinium Oxide and Gold Hybrid Nanoparticles. ACS Appl Bio Mater. 2023 Feb;6(2):784–792. PMID: 36693820. Available from: https://doi.org/10.1021/acsabm.2c00965.
- Zhang NN, Lu CY, Chen MJ, Xu XL, Shu GF, Du YZ. Recent advances in near-infrared II imaging technology for biological detection. J Nanobiotechnology. 2021 May;19(1):132. PMID: 33971910. Available from: https://doi.org/10.1186/s12951-021-00870-7.
- Zhang Y, Li Z, Du Z, Pan J, Huang Y. Multifunctional Upconversion Nanoparticles Transforming Photoacoustic Imaging: A Review. Nanomaterials (Basel). 2025 Jul;15(14):1074.
   PMID: 40711193. Available from: https://doi.org/10.3390/ nano15141074.
- Zhao S, Tian R, Shao B, Feng Y, Yuan S, Dong L. UCNP-Bi2Se3 Upconverting Nanohybrid for Upconversion Luminescence and CT Imaging and Photothermal Therapy. Chemistry. 2020 Jan;26(5):1127–1135. PMID: 31721326. Available from: https://doi.org/10.1002/chem.201904586.
- 122. Ferro-Flores G, Ancira-Cortez A, Ocampo-García B, Meléndez-Alafort L. Molecularly Targeted Lanthanide Nanoparticles for Cancer Theranostic Applications. Nanomaterials (Basel). 2024 Jan;14(3):296. PMID: 38334567. Available from: https://doi.org/10.3390/nano14030296.
- Zhang Q, O'Brien S, Grimm J. Biomedical Applications of Lanthanide Nanomaterials, for Imaging, Sensing and Therapy. Nanotheranostics. 2022 Jan;6(2):184–194. PMID:

- 34976593. Available from: https://doi.org/10.7150/ntno.65530.
- 124. Li X, Jiang M, Zeng S, Liu H. Polydopamine coated multifunctional lanthanide theranostic agent for vascular malformation and tumor vessel imaging beyond 1500 nm and imaging-guided photothermal therapy. Theranostics. 2019 May;9(13):3866-3878. PMID: 31281519. Available from: https://doi.org/10.7150/thno.31864.
- 125. Jiang X, Jiang X, Wu D, Xie W, Liu X, Zheng J. A pH-Sensitive Nanoparticle as Reactive Oxygen Species Amplifier to Regulate Tumor Microenvironment and Potentiate Tumor Radiotherapy. Int J Nanomedicine. 2024 Jan;19:709–725. PMID: 38283195. Available from: https://doi.org/10.2147/IJN. \$435160.
- Carofiglio M, Barui S, Cauda V, Laurenti M. Doped Zinc Oxide Nanoparticles: Synthesis, Characterization and Potential Use in Nanomedicine. Appl Sci (Basel). 2020 Jul;10(15):5194.
   PMID: 33850629. Available from: https://doi.org/10.3390/app10155194.
- 127. Lux F, Tran VL, Thomas E, Dufort S, Rossetti F, Martini M. AGulX® from bench to bedside—Transfer of an ultrasmall theranostic gadolinium-based nanoparticle to clinical medicine. Br J Radiol. 2019 Jan;92(1093). PMID: 30226413. Available from: https://doi.org/10.1259/bjr.20180365.
- 128. Verry C, Dufort S, Villa J, Gavard M, Iriart C, Grand S. Theranostic AGulX nanoparticles as radiosensitizer: A phase I, dose-escalation study in patients with multiple brain metastases (NANO-RAD trial). Radiother Oncol. 2021 Jul;160:159–165. PMID: 33961915. Available from: https://doi.org/10.1016/i.radonc.2021.04.021.
- Luo Y. Radiobiological perspective on metrics for quantifying dose enhancement effects of High-Z nanoparticles. Front Nanotechnol. 2025;7. Available from: https://doi.org/10.3389/ fnano.2025.1603334.
- Lu VM, Crawshay-Williams F, White B, Elliot A, Hill MA, Townley HE. Cytotoxicity, dose-enhancement and radiosensitization of glioblastoma cells with rare earth nanoparticles. Artif Cells Nanomed Biotechnol. 2019 Dec;47(1):132– 143. PMID: 30663430. Available from: https://doi.org/10.1080/ 21691401.2018.1544564.
- Zhong D, Wang Y, Xie F, Chen S, Yang X, Ma Z. A biomineralized Prussian blue nanotherapeutic for enhanced cancer photothermal therapy. J Mater Chem B. 2022 Jun;10(25):4889–4896. PMID: 35699145. Available from: https://doi.org/10.1039/D2TB00775D.
- 132. Fuentealba M, Ferreira A, Salgado A, Vergara C, Díez S, Santibáñez M. An Optimized Method for Evaluating the Potential Gd-Nanoparticle Dose Enhancement Produced by Electronic Brachytherapy. Nanomaterials (Basel). 2024 Feb;14(5):430. PMID: 38470761. Available from: https://doi.org/10.3390/nano14050430.
- 133. Chen ZH, Wang X, Yang M, Ming J, Yun B, Zhang L. An Extended NIR-II Superior Imaging Window from 1500 to 1900 nm for High-Resolution In Vivo Multiplexed Imaging Based on Lanthanide Nanocrystals. Angew Chem Int Ed Engl. 2023 Dec;62(49). PMID: 37860881. Available from: https://doi.org/10.1002/anie.202311883.
- Tsang CY, Zhang Y. Nanomaterials for light-mediated therapeutics in deep tissue. Chem Soc Rev. 2024 Mar;53(6):2898–2931. PMID: 38265834. Available from: https://doi.org/10.1039/D3CS00862B.
- 135. Aloy MT, Sidi Boumedine J, Deville A, Kryza D, Gauthier A, Brichart-Vernos D. Proof of Concept of the Radiosensitizing Effect of Gadolinium Oxide Nanoparticles in Cell Spheroids and a Tumor-Implanted Murine Model of Chondrosarcoma. Int J Nanomedicine. 2022 Dec;17:6655–6673. PMID: 36582458. Available from: https://doi.org/10.2147/IJN.S390056.
- 136. Li B, Zhao M, Lin J, Huang P, Chen X. Management of fluorescent organic/inorganic nanohybrids for biomedical applications in the NIR-II region. Chem Soc Rev. 2022 Sep;51(18):7692–7714. PMID: 35861173. Available from: https: //doi.org/10.1039/D2CS00131D.
- 137. Khan IĂ, Yu T, Yang M, Liu J, Chen Z. A Systematic Re-

- view of Toxicity, Biodistribution, and Biosafety in Upconversion Nanomaterials: Critical Insights into Toxicity Mitigation Strategies and Future Directions for Safe Applications. BME Frontiers. 2025;6. Available from: https://doi.org/10.34133/bmef.0120.
- Funke SK, Factor C, Rasschaert M, Lezius L, Sperling M, Karst U. Long-term Gadolinium Retention in the Healthy Rat Brain: Comparison between Gadopiclenol, Gadobutrol, and Gadodiamide. Radiology. 2022 Oct;305(1):179–189. PMID: 35727155. Available from: https://doi.org/10.1148/radiol.212600.
- Li Z, Gong J, Lu S, Li X, Gu X, Xu J. Photothermal lanthanide nanomaterials: from fundamentals to theranostic applications. BMEmat. 2024;2(4). Available from: https://doi.org/ 10.1002/bmm2.12088.
- 140. Tian C, Xue X, Chen Y, Liu R, Wang Y, Ye S. Phosphotungstate Acid Doped Polyanilines Nanorods for in situ NIR-II Photothermal Therapy of Orthotopic Hepatocellular Carcinoma in Rabbit. Int J Nanomedicine. 2022 Nov;17:5565–5579. PMID: 36444199. Available from: https://doi.org/10.2147/IJN. S380370.
- 141. Cao T, Yang Y, Sun Y, Wu Y, Gao Y, Feng W. Biodistribution of sub-10 nm PEG-modified radioactive/upconversion nanoparticles. Biomaterials. 2013 Sep;34(29):7127-7134. PMID: 23796579. Available from: https://doi.org/10.1016/j.biomaterials.2013.05.028.
- 142. Zhang H, Wang X, Jin R, Su Q. Preparation and applications of polymer-modified lanthanide-doped upconversion nanoparticles. Giant (Oxf). 2022;12:100130. Available from: https://doi.org/10.1016/j.giant.2022.100130.
- 143. Li Q, Wang Z, Chen Y, Zhang G. Elemental bio-imaging of PEGylated NaYF4:Yb/Tm/Gd upconversion nanoparticles in mice by laser ablation inductively coupled plasma mass spectrometry to study toxic side effects on the spleen, liver and kidneys. Metallomics. 2017 Aug;9(8):1150–1156. PMID: 28745365. Available from: https://doi.org/10.1039/ C7MT00133K.
- 144. Yu J, Yin W, Peng T, Chang YN, Zu Y, Li J. Biodistribution, excretion, and toxicity of polyethyleneimine modified NaYF4:Yb,Er upconversion nanoparticles in mice via different administration routes. Nanoscale. 2017 Mar;9(13):4497–4507. PMID: 28317980. Available from: https://doi.org/10.1039/C7NR00078B.
- 145. Fretellier N, Idée JM, Rasschaert M, Factor C, Van der Molen AJ. Gadolinium Deposition in Bone Tissues After Contrast-enhanced Magnetic Resonance Imaging: A Comprehensive Review. Invest Radiol. 2025 Nov;60(11):722–744. PMID: 40574249. Available from: https://doi.org/10.1097/RLI. 00000000000001208.
- 146. Biau J, Durando X, Boux F, Molnar I, Moreau J, Leyrat B. NANO-GBM trial of AGuIX nanoparticles with radiotherapy and temozolomide in the treatment of newly diagnosed Glioblastoma: Phase 1b outcomes and MRI-based biodistribution. Clin Transl Radiat Oncol. 2024 Jul;48. PMID: 39184998. Available from: https://doi.org/10.1016/j.ctro.2024.100833.
- 147. lacobellis F, Di Serafino M, Russo C, Ronza R, Caruso M, Dell'Aversano Orabona G. Safe and Informed Use of Gadolinium-Based Contrast Agent in Body Magnetic Resonance Imaging: Where We Were and Where We Are. J Clin Med. 2024 Apr;13(8):2193. PMID: 38673466. Available from: https://doi.org/10.3390/jcm13082193.
- Seo HJ, Nam SH, Im HJ, Park JY, Lee JY, Yoo B. Rapid Hepatobiliary Excretion of Micelle-Encapsulated/Radiolabeled Upconverting Nanoparticles as an Integrated Form. Sci Rep. 2015 Oct;5(1):15685. PMID: 26494465. Available from: https://doi.org/10.1038/srep15685.
- Mi P. Stimuli-responsive nanocarriers for drug delivery, tumor imaging, therapy and theranostics. Theranostics. 2020 Mar;10(10):4557–4588. PMID: 32292515. Available from: https://doi.org/10.7150/thno.38069.
- 150. Chen H, Timashev P, Zhang Y, Xue X, Liang XJ. Nanotechnology-based combinatorial phototherapy

- for enhanced cancer treatment. RSC Adv. 2022 Apr;12(16):9725–9737. PMID: 35424935. Available from: https://doi.org/10.1039/D1RA09067D.
- 151. Zhang Y, Zhang G, Wang G, Wu L, Monteiro-Riviere NA, Li Y. The synergistic strategies for the immuno-oncotherapy with photothermal nanoagents. Wiley Interdiscip Rev Nanomed Nanobiotechnol. 2021 Sep;13(5). PMID: 33825343. Available from: https://doi.org/10.1002/wnan.1717.
- 152. Rahmani AA, Jia Q, Bahti HH, Fauzia RP, Wyantuti S. Recent advances in lanthanide-based nanoparticle contrast agents for magnetic resonance imaging: Synthesis, characterization, and applications. OpenNano. 2025;21:100226. Available from: https://doi.org/10.1016/j.onano.2024.100226.
- 153. Zhang J, Du J, Jia S, Li Y, Ågren H, Prasad PN. Recent Advances in Upconversion Nanoparticles for Therapeutics: From Fundamentals to Cutting-Edge Applications. Electron. 2025;3(3). Available from: https://doi.org/10.1002/elt2.70012.
- Luo Z, Mao D, Li X, Luo J, Gong C, Liu X. Lanthanide-based nanoparticles for cancer phototherapy. Coord Chem Rev. 2024;508:215773. Available from: https://doi.org/10.1016/j.ccr. 2024.215773.
- 155. Wu X, Chen G, Shen J, Li Z, Zhang Y, Han G. Upconversion nanoparticles: a versatile solution to multiscale biological imaging. Bioconjug Chem. 2015 Feb;26(2):166–175. PMID: 25254658. Available from: https://doi.org/10.1021/bc5003967.
- Zhao M, Chen X. Recent Advances in NIR-II Materials for Biomedical Applications. Acc Mater Res. 2024;5(5):600–613.
   Available from: https://doi.org/10.1021/accountsmr.4c00025.
- Lei X, Li R, Tu D, Shang X, Liu Y, You W. Intense near-infrared-II luminescence from NaCeF4:Er/Yb nanoprobes for *in vitro* bioassay and *in vivo* bioimaging. Chem Sci (Camb).
   May;9(20):4682–4688. PMID: 29899962. Available from: https://doi.org/10.1039/C8SC00927A.
- 158. Guo Y, Hu J, Wang P, Yang H, Liang S, Chen D. In Vivo NIR-II Fluorescence Lifetime Imaging of Whole-Body Vascular Using High Quantum Yield Lanthanide-Doped Nanoparticles. Small. 2023 Aug;19(35). PMID: 37127883. Available from: https://doi.org/10.1002/smll.202300392.
- 159. Wang Q, Zhang X, Tang Y, Xiong Y, Wang X, Li C. High-Performance Hybrid Phototheranostics for NIR-IIb Fluorescence Imaging and NIR-II-Excitable Photothermal Therapy. Pharmaceutics. 2023 Jul;15(8):2027. PMID: 37631241. Available from: https://doi.org/10.3390/pharmaceutics15082027.
- 160. Wen HQ, Peng HY, Liu K, Bian MH, Xu YJ, Dong L. Sequential Growth of NaYF4:Yb/Er@NaGdF4 Nanodumbbells for Dual-Modality Fluorescence and Magnetic Resonance Imaging. ACS Appl Mater Interfaces. 2017 Mar;9(11):9226–9232. PMID: 28244317. Available from: https://doi.org/10.1021/acsami.6b16842.
- 161. Zhang Z, Sheng J, Zhang M, Ma X, Geng Z, Wang Z. Dual-modal imaging and excellent anticancer efficiency of cisplatin and doxorubicin loaded NaGdF4:Yb3+/Er3+ nanoparticles. RSC Adv. 2018 Jun;8(39):22216–22225. PMID: 35541744. Available from: https://doi.org/10.1039/C8RA03898H.
- 162. Liu C, Gao Z, Zeng J, Hou Y, Fang F, Li Y. Mag-

- netic/upconversion fluorescent NaGdF4:Yb,Er nanoparticle-based dual-modal molecular probes for imaging tiny tumors in vivo. ACS Nano. 2013 Aug;7(8):7227–7240. PMID: 23879437. Available from: https://doi.org/10.1021/nn4030898.
- 163. Yang Y, Tu D, Zhang Y, Zhang P, Chen X. Recent advances in design of lanthanide-containing NIR-II luminescent nanoprobes. iScience. 2021 Jan;24(2):102062. PMID: 33604522. Available from: https://doi.org/10.1016/j.isci.2021.102062.
- 164. Jeong S, Won N, Lee J, Bang J, Yoo J, Kim SG. Multiplexed near-infrared in vivo imaging complementarily using quantum dots and upconverting NaYF4:Yb3+,Tm3+ nanoparticles. Chem Commun (Camb). 2011 Jul;47(28):8022–8024. PMID: 21660354. Available from: https://doi.org/10.1039/c1cc12746b.
- 165. Sun Y, Peng J, Feng W, Li F. Upconversion nanophosphors NaLuF4:Yb,Tm for lymphatic imaging in vivo by real-time upconversion luminescence imaging under ambient light and high-resolution X-ray CT. Theranostics. 2013 Apr;3(5):346– 353. PMID: 23650481. Available from: https://doi.org/10.7150/ thno.5137.
- 166. Zhu X, Zhang H, Zhang F. Expanding NIR-II Lanthanide Toolboxes for Improved Biomedical Imaging and Detection. Acc Mater Res. 2023;4(6):536–547. Available from: https://doi.org/10.1021/accountsmr.2c00117.
- 167. Guo Y, Hu J, Wang P, Yang H, Liang S, Chen D. In Vivo NIR-II Fluorescence Lifetime Imaging of Whole-Body Vascular Using High Quantum Yield Lanthanide-Doped Nanoparticles. Small. 2023 Aug;19(35). PMID: 37127883. Available from: https://doi.org/10.1002/smll.202300392.
- 168. Zhu YY, Song L, Zhang YQ, Liu WL, Chen WL, Gao WL. Development of a Rare Earth Nanoprobe Enables In Vivo Real-Time Detection of Sentinel Lymph Node Metastasis of Breast Cancer Using NIR-IIb Imaging. Cancer Res. 2023 Oct;83(20):3428–3441. PMID: 37540231. Available from: https://doi.org/10.1158/0008-5472.CAN-22-3432.
- 169. Sun Z, Huang H, Zhang R, Yang X, Yang H, Li C. Activatable Rare Earth Near-Infrared-II Fluorescence Ratiometric Nanoprobes. Nano Lett. 2021 Aug;21(15):6576–6583. PMID: 34304558. Available from: https://doi.org/10.1021/acs.nanolett.1c01962.
- 170. Hong M, Sun P, Liu Y, Ke J, Wu Z. Lanthanide-based NIR-II Fluorescent Nanoprobes and Their Biomedical Applications. Huaxue Xuebao. 2022;80(4):542. Available from: https://doi. org/10.6023/A21120571.
- 171. Lv K, Wang H, Fu X, Chen S, Zhang R, Zhou Y. An Integrated Nanoplatform via Dual Channel Excitation for Both Precise Fluorescence Imaging and Photodynamic Therapy of Orthotopic Breast Tumor in NIR-II Region. Small. 2024 Nov;20(47). PMID: 39140318. Available from: https://doi.org/10.1002/smll. 202404007.
- 172. Duan G, Zhang J, Wei Z, Wang X, Zeng J, Wu S. Intraoperative diagnosis of early lymphatic metastasis using neodymium-based rare-earth NIR-II fluorescence nanoprobe. Nanoscale Adv. 2023 Jul;5(16):4240–4249. PMID: 37560436. Available from: https://doi.org/10.1039/D3NA00254C.